UNIVERSITÀ DEGLI STUDI DI CATANIA
DIPARTIMENTO DI INGEGNERIA ELETTRICA, ELETTRONICA ED INFORMATICA

DOTTORATO DI RICERCA IN INGEGNERIA INFORMATICA E DELLE TELECOMUNICAZIONI
XXVI CICLO

INTRODUCING COMMUNICATION AND NETWORKING TECHNOLOGIES INTO LAB-ON-CHIP SYSTEMS

ING. ELENA DE LEO

Coordinatore	Tutor
Chiar.ma Prof. V. CARCHIOLO	Chiar.mo Prof. G. MORABITO

to my family and friends, always present in my life

CONTENTS

LIST OF FIGURES

LIST OF TABLES

ABSTRACT

Microfluidics is a science and a technology which deals with manipulation and control of small volumes of fluids flowing in channels of micro-scale size. It is currently used for Labs-On-a-Chip (LoCs) applications mainly. In this context, recently fluids have been used in the discrete form of droplets or bubbles dispersed into another immiscible fluid. In this case, droplets or bubbles can be exploited as a means to transport digital information between microfluidic components, with sequences of particles (i.e. droplets or bubbles) representing sequences of binary values. LoCs are today realized through monolithic devices in which samples are processed by passing them through a predetermined sequence of elements connected by fixed and preconfigured microfluidic channels. To increase reusability of LoCs, effectiveness and flexibility, networking functionalities can be introduced so that the sequence of elements involved in the processing can be dynamically selected. Accordingly, in this thesis we introduce the Networked LoC (NLoC) paradigm that brings networking concepts and solutions in microfluidic systems such as LoCs. More specifically, in this paper the need for the introduction of the NLoC paradigm is motivated, its required functions are identified, a system architecture is proposed, and the related physical level design aspects, such as

channel characterization, information representation and information capacity are investigated; finally a switching device is proposed and studied.

CHAPTER

ONE

INTRODUCTION

In the recent years the use of on-chip technologies for chemical and biomedical environments has increased significantly: it is usually referred to as *Labs-on-a-Chip* (LoC) technology, meaning that different laboratory functions are executed on a single chip, usually fabricated with or various polymers such as polydimethylsiloxane (PDMS) and polycarbonate or glass, plastic, silicon and small in size (from few mm^2 to cm^2). Such technology allows LoCs to perform extremely complex operations in devices of small size. As an example of a LoC component, in Figure 1.1 a scheme of an on-chip microreactor is shown [1]; a microreactor is a small size chip in which several substances (the reagents) are injected and then processed in order to perform a desired chemical reaction; the labels A1, A2 and A3 in Figure 1.1 show the inlets through which reagents are introduced in the device. After having been injected in the circuit, such reagents move along a tortuous path: this movement mixes them, thus resulting in a chemical reaction. LoCs can be used in several contexts, they require small amounts of reagents, in the order of few μl to pl, and their

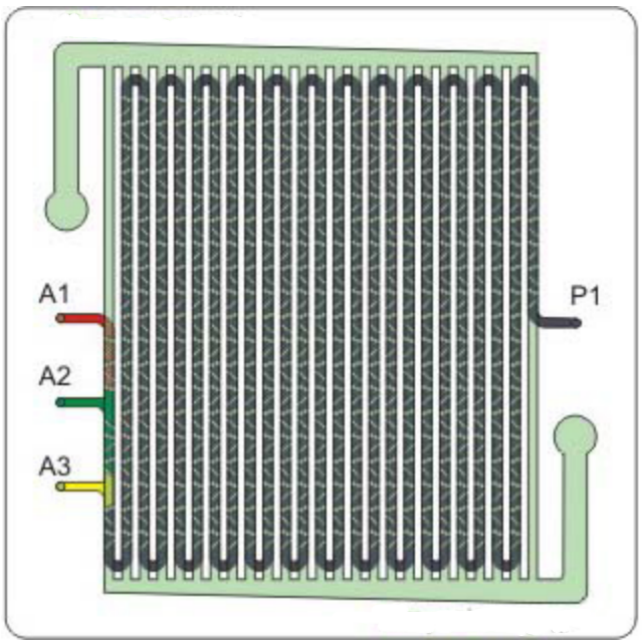

Figure 1.1: A microfluidic microreactor (reproduced from [1]).

cost is low. Regardless of such advantages, their place in the market is still quite limited, mainly due to their lack of flexibility [5] [6].

We argue that an increase in flexibility can be achieved by introducing some basic networking functionalities in LoCs systems.

Before moving on to the next sections, let us take a step back and give a brief overview of *microfluidics*, the branch of physics on which LoC technologies rely.

1.1 Microfluidics

Microfluidics is both a science and a technology [7] that deals with the control of small amounts of *fluids* flowing through micro-channels, with sizes in the order of μm. At such scale, systems exhibit the following features:

- **Small size**: Microfluidic systems have small size and deal with very small samples. This is in contrast with current chemical analysis/synthesis that is often realized over large samples.

- **Reversibility and**, to some extent, **predictability**: At macro-scale, fluids move in a turbulent way. At micro-scale the flow is laminar due to inertia and pressure. If such fluids are incompressible (i.e. their densities do not vary with time and space), then the system is *reversible* and controllable.

Applications of microfluidics span over a wide range of domains going from inkjet printheads to DNA chips, from micro-propulsion to micro-thermal technologies.

We are interested in droplets microfluidics which is related to the control of the motion dynamics of droplets into microchannels[1]. In this scenarios, droplets are dispersed into another fluid, which is immiscible with them. This kind of mixtures are generically named *dispersions* and droplets are technically called *dispersed phase*, while the immiscible substance, in which they are immersed, is called *continuous phase*. Current microfluidic technologies allow control of shape, motion and size of particles dispersed in a continuous phase.

[1] In the following we will usually refer to droplets; however, the same can be applied if the emulsion is in gaseous state, i.e., in the form of bubbles.

Droplet microfluidics can be applied to biological as well as chemical analysis and synthesis. Indeed, it is straightforward thinking to microfluidic systems as an effective tool to transport samples (for instance by means of droplets), in order to make them interact with appropriate substances in highly controlled conditions, and to realize tasks that are common in chemical analysis, with high resolution, sensitivity and precision. In other words droplet microfluidics can be seen as the basic building block of *labs-on-a-chip*. Recently several approaches have been proposed to control the movements of droplets into microfluidic systems. Examples include pure hydrodynamic manipulation (HM), electrohydrodynamic manipulation (EM), thermocapillary manipulation (TM), magnetic manipulation (MM) and acoustic manipulation (AM), based on the following physical principles:

- in hydrodynamic manipulation, geometries of the channels and hydrodynamic forces are used to move droplets along a sequence of channels;
- by electrohydrodynamic manipulation, conductive droplets are driven along desired paths by appropriately acting on a grid of electrodes;
- in magnetic manipulation, droplets containing magnetic beads are driven by a magnetic field;
- in thermocapillary manipulation, droplets are driven by a temperature gradient, exploiting the – so called – Marangoni effect;
- in acoustic manipulation, acoustic waves are used to modify internal streaming of a fluid.

AM, MM and TM are very sensitive to noise. EM, instead, is still expensive and complex. On the contrary, HM is simple to realize and cost effective.

So, a significant branch of research focuses on this approach. Recents studies have extended the previous preliminary work on HM in microchannels [8] by introducing the innovative concept of *"bubble logic"* [9, 10] which consists of steering hydrodynamically the flow of droplets into a network of microchannels by means of other properly timed droplets. These aspects will be described in detail in Chapter 2.3.

1.2 Motivation and basic idea

LoCs integrate several microfluidic elements able to perform specific laboratory functions in a single chip. Such structure allows LoCs to perform extremely complex operations in devices of small size. Currently, LoCs are realized as monolithic devices in which samples are processed by passing them through a predefined and ordered sequence of elements.

On the contrary, the cost of LoCs could be reduced, their reusability increased and their effectiveness improved by providing more flexibility. Indeed, if LoCs can select the sequence of elements to be involved in the processing of a given sample in a programmable and adaptive way, then it is possible to use the same LoC system to perform different tasks (even simultaneously) and to modify the process, if required.

In traditional microfluidic systems this is not feasible because the output of a given element is statically connected by microfluidic channels to the input of another element and therefore the sequence of elements that will be traversed by any sample is built in the topology of the LoC device. To overcome this limitation, networking technologies can be integrated in LoC systems. We denote the resulting system as *Networked Lab-On-a-Chip* (NLoC).

1.3 Contributions

It is intuitive that huge research effort is needed to identify and solve the paramount number of open issues involved by the introduction of the NLoC paradigm. In this thesis we address the main networking issues related to microfluidic networking. Indeed, specific contributions of this thesis are the following:

1. We introduce the NLoC concept, identify the required functions and provide the related design guidelines. To this purpose we will provide the basics of microfluidics using a language and a perspective as close as possible to that of the scientists belonging to the computer and communications engineering communities. [11] [12] [13]

2. We propose a system architecture that is in line with the design guidelines mentioned above. [11] [12] [13]

3. We investigate how to represent information in NLoCs. Different approaches are discussed and the most promising are analyzed and compared. [11] [12] [13]

4. We provide a preliminary characterization of microfluidic channels in the perspective of information capacity evaluation. [11] [12] [13]

5. We define a solution for a passive microfluidic switch which can be used to route droplets in the microfluidic network [14] [15] [16] [17]

The rest of this thesis is organized as follows. In Chapter 2 a thorough discussion on the basics of droplet microfluidic technologies which are used in the rest of the paper is provided. In Chapter 3 we introduce the NLoC concept,

discuss a few architectural options and compare their advantages and disadvantages. Information capacity and its representation in such environments will be discussed in Chapter 4. In Chapter 5 the *Hydrodynamic Controlled Microfluidic Network* (HCN) paradigm is proposed, which is based on a pure hydrodynamic microfluidic switching function. In Chapters 7 and 6 simulation and prototype experimental results are presented in order to assess the feasibility of the HCN paradigm. Finally, Chapter 8 provides some concluding remarks.

CHAPTER

TWO

MICROFLUIDIC TECHNOLOGIES: THEORY, RESEARCH TOOLS AND STATE OF THE ART

In this chapter, we provide an overview of the theoretical background required to understand the physical concepts that are at the base of microfluidic computing and communications. Such overview is reported in Section 2.1. Then, in Section 2.2 we provide a brief survey of the most relevant techniques for droplet generation and manipulation in the area of microfluidic technologies. In Section 2.3 we report the most relevant results in the area of microfluidic computing and communications. Finally, in Section 2.4 we describe the most popular research tools utilized in microfluidic research.

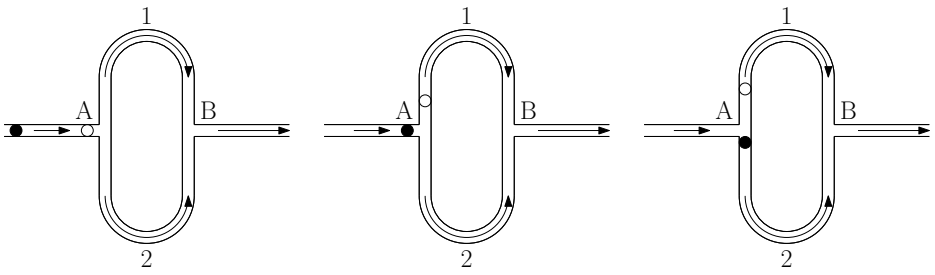

Figure 2.1: Droplets motion in a bi-phase flow: a) first droplet arrival b) second droplet arrival c) second droplet transition.

2.1 Introduction to hydrodynamic microfluidics for non physicists

A thorough introduction to droplet microfluidics can be found in [9,18,19]. In the following, we summarize the aspects that are more relevant to our work.

Consider a micro scale cylindrical pipe of length L and diameter of cross-section D where a fluid flows with average velocity v. The flux Q is the volume of fluid traversing any boundary, i.e. cross-section, of the pipe in a unit of time and can be calculated as

$$Q = v\pi R^2 \tag{2.1}$$

where $R = D/2$ is the pipe radius. The value of the flux Q depends on the pressure difference at the ends of the pipe, ΔP. In fact it can be observed that [9]:

$$\frac{\Delta P}{Q} \approx \frac{\mu L}{D^4} \tag{2.2}$$

where μ is the viscosity of the flow.

When we consider a channel in which droplets are introduced, the dynamic nature of the fluid motion inside the pipe changes in a non-linear and history-dependent way: since the dispersed phase and the continuous phase are immiscible, a droplet inside the pipe acts like an obstacle or a plug in the main flow; this introduces an additional resistance to the flow. This additional resistance can be modeled as an additive pressure drop given by

$$\Delta P_{Ca} \approx \frac{\sigma}{R} Ca^{\frac{2}{3}} \tag{2.3}$$

where σ is the surface tension between the two phases and

$$Ca = \frac{\mu v}{\sigma} \tag{2.4}$$

is the *Capillary number* which is a flow dynamic parameter such that a variation of Ca within a given range guarantees to have a good control over the droplet motion. The dependence on the presence of droplets leads the system to have complex dynamics.

Let us consider now a more complex system, where a bi-phase flow moves through a pipe. Then the pipe divides into two branches, which then merge in a new pipe, as shown in Figure 2.1. The lengths of the two branches differ by little percentage, and the pipes have the same section. Accordingly, the pressure drop between A and B is the same for the two pipes, but the hydrodynamic resistance of the shorter branch (i.e. branch 1) is smaller than the one of the longer branch (i.e. branch 2).

Let $R_1(n_{d_1})$ and $R_2(n_{d_2})$ be the hydraulic resistances of pipes 1 and 2, respectively, when there are n_{d_1} droplets in branch 1 and n_{d_2} droplets in branch 2, that is the resistance of pipe i depends on the presence of n_{d_i} droplets inside it.

A droplet arriving at the T-shaped bifurcation in Figure 2.1, denoted as A, will always follow the branch with the smaller resistance: if the shorter

branch is empty, the droplet will certainly flow through this branch because $R_1(0) < R_2(0)$. As an example in Figure 2.1a the first droplet (the white one) goes into the branch 1 because it is empty and it is the path of least resistance. When a second droplet (the black one) arrives at point A, as shown in Figure 2.1b, the resistance of pipe 1 will be $R_1(1) > R_1(0)$ because the first droplet already entered branch 1; if $R_1(1) > R_2(0)$ then the second droplet arriving at A will follow branch 2 as shown in Figure 2.1c, thus increasing its resistance to a greater value $R_2(1)$.

Of course if the relationship $\min\{n_{d_1} : R_1(n_{d_1}) > R_2(0)\} \geq 1$ holds, then more than one droplet is necessary in pipe 1 in order to deviate the successive droplet through pipe 2 when it is assumed to be empty. So the path that a droplet travels between A and B depends on the past history of the channel which introduces complex dynamics [20]. This behavior is relevant in droplet microfluidics, because the geometry of bifurcation A as in Figure 2.1 is the most common way to connect pipes in microfluidic circuits.

2.2 Droplet generation and manipulation

Networked Lab-on-a-Chip require high control over motion, size, distance and interaction between small amount of fluids. In droplet microfluidics several ways to manipulate droplets have been devised [21]. In this section we provide an overview of the techniques that implement droplet generation and manipulation.

A list of common operations performed on droplets is given below:

- *Generation of droplet*: this is the first step of droplet manipulation: generating droplets of desired size, distance and shape is a basic requirement of all microfluidic applications and is related to information cod-

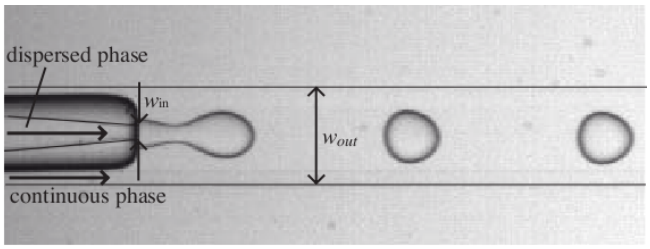

Figure 2.2: Microfluidic device generating droplets by means of a coaxial geometry (reproduced from [2]).

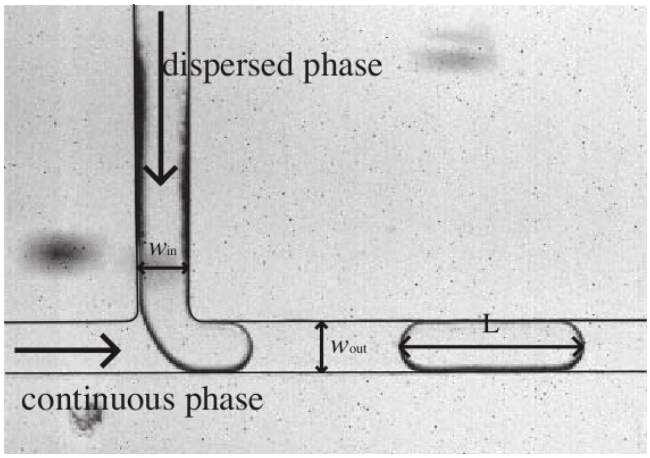

Figure 2.3: Microfluidic device generating droplets by means of a T-junction geometry (reproduced from [3]).

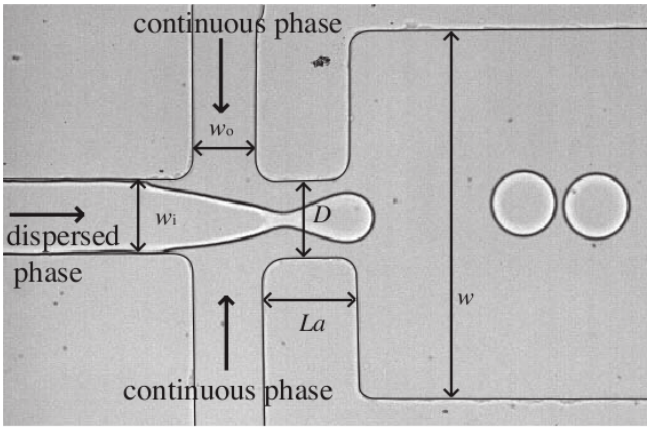

Figure 2.4: Microfluidics device generating droplets by means of a flow-focusing mechanism (reproduced from [3]).

ing in the NLoC system. Several devices exist which implement this task [2]. In Figures 2.2, 2.3 and 2.4 such kind of devices are shown.

- *Fission*: droplets can be split to increase system capacity. In fact, each droplet can be a vessel for various reagents. Accordingly, droplet fission can help to increase system capacity. However, fission of one or more droplets into new droplets may be an undesired event in case of presence or distance encoding: in fact this would lead the receiver to misinterpret a sequence of droplets, thus raising an error in the decoding process. This can be controlled by choosing the substance composing the droplets with an appropriate viscosity, to make them remain cohesive.

- *Fusion*: it is needed in tasks in which the bubbles/droplets work as microreactors, i.e. they transport chemical/biological reagents within themselves and it is critical that they merge when given conditions oc-

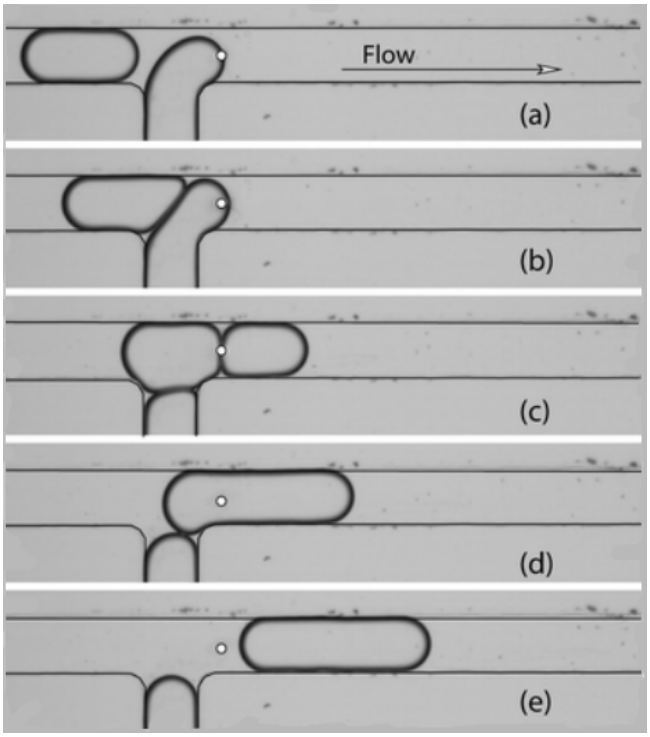

Figure 2.5: Fusion of two droplets forced by a laser beam (reproduced from [4]).

cur. So fusion is related to the payload "processing" in the NLoC environment. This can be achieved, for instance, by applying to the flow a temperature gradient by means of a laser beam: as shown in Figure 2.5 a laser beam is capable of blocking the interface between the continuous and the dispersed phase; when the second droplet arrives, the interface of the first droplet pushes on the second droplet until they merge and overcome the pressure given by the laser beam. Similarly to the case of fission, also fusion can cause errors in the decoding process. As previously mentioned, this can be avoided by properly choosing the time interval between consecutive droplets.

- *Motion*: motion of droplets must be controlled and exploited to make droplets flow through programmed paths. This is currently the most challenging aspect of droplet microfluidics and is strongly related to the internetworking capability of the NLoC.

Motion can be implemented by means of various techniques of manipulation, other than the hydrodynamic manipulation which is the one we propose to employ in our NLoC case as discussed in Section 1.1.

2.3 Microfluidic computing and communications

Recently the idea to process and transfer information by means of fluid motion has been proposed [22] [8] [23].
As in the context of conventional computing, also in this case hardware devices have been designed which perform simple atomic operations. Thus, a microfluidic device is atomic in the hardware. Prakash et al. [22] realized and tested devices which implement some common logical and timing functions: a) a binary AND-OR gate b) a T flip-flop, c) a droplet synchronizer and d)

an oscillator. The AND-OR gate and the T flip-flop are based on an information encoding mechanism based on presence/absence coding: a droplet in the channel can be identified with a binary value 1 while no droplets in the channel corresponds to binary value 0. Existence of AND-OR and NOT microfluidic functions is a fundamental issue since it is well known that AND, OR and NOT-gates are a functionally complete operator set, so any binary operation can be implemented through a combination of those gates. A flip-flop can be used as a buffer while the oscillator is capable of making a droplet circulate in a circular pipe with a given periodicity. Finally, the synchronizer is a circuit with two inputs and two outputs. Two droplets, each entering from a different entrance with a certain time displacement, are aligned while they traverse the device, so that they exit at the same time.

Also some solutions for encoding/decoding information through microfluidic circuits have been proposed in [8]. They typically exploit a cascade of two loops like those illustrated in Figure 2.1. There it is evident that the two loops should exhibit the same topology in order to allow reconstruction of the information at the destination. This approach to information encoding is based on tuning the distance between the droplets entering the loop. This can be achieved by appropriately setting the flow rate of the dispersed phase and continuous phase, thus resulting in a range of frequencies at which droplets are generated.

When a train of equally spaced droplets goes through the loop, the complex dynamics described in Section 2.1 arise. As a result the sequence of droplets at the output of the loop is not equally spaced anymore. However a regularity has been observed in them: there is a pattern of distances between consecutive droplets that repeats in time, after a certain number of droplets has passed through the loop. It has also been observed that different patterns at the output of the loop are associated with the frequency at which droplets are generated

at the input. In order to reconstruct the initial information, it is necessary that a twin microfluidic loop is used at destination to properly reconstruct the initial distance between droplets, i.e., information is carried in the distance between droplets. Accordingly, these approaches can be also considered for cryptography.

2.4 Computational fluid dynamics and simulation tools

NLoC system design needs for analysis of the droplets' motion mechanisms in a microfluidic system. To this purpose, several - often integrated - approaches can be considered:

1. Experimentation in microfluidic devices is often the most simple (and accurate) manner to achieve such goal.

2. When experimental study is not possible or too costly, mathematical models can be used. Usually they consist of partial differential equations (PDE). Unfortunately, the resulting system of equations is extremely complex and, in general, it is not possible to find closed form solutions. Alternatively, in order to identify mathematical models, analogies between microfluidic and electrical circuits can be exploited as proposed in [9, 10, 24–26]. In this case, a pressure drop between two different points of a pipe can be identified with a voltage variation; a volumetric flux can be seen as an electrical current and a fluid resistance is the analogous of an electrical resistance.

3. When the analytical solution to the above equations cannot be found, specific software tools can be used. In fact, several software tools exist

that numerically solve PDEs, making use of effective and low resource-consuming algorithms.

In the following we focus on such software tools, that have become effective only when powerful computers have been realized. The types of software that are most commonly used nowadays for microfluidic computation are given below:

- COMSOL [27]: this is a commercial software with a modular structure. Each package is dedicated to a specific physical branch, including microfluidics. It implements several algorithms and solvers which numerically solve PDE for a given physical set-up, by means of the Finite Element Method (FEM).
  In its simplest configuration, COMSOL has a very intuitive graphical user interface, including i) a simple CAD interface that can be used to describe the geometry and the physics of the investigated system, ii) a tool for setting the options to be used for the numerical solution of the PDE and iii) several tools for pre- and post-processing of the results. The resulting environment provides a user friendly working experience. COMSOL is a software developed from Matlab: as a consequence, a specific package exists which links COMSOL mathematical results (matrices and files) to Matlab. This makes it possible to realize custom postprocessing operations with Matlab.
  Major disadvantages are the following: since it is a commercial software, the number of simulations that can be executed in parallel is limited by the number of available licenses. Moreover, similarly to other multiphysics simulators, it is resource demanding: the parameter which mostly affects its performance is the amount of RAM installed on the machine. For the configurations we studied, the minimum amount of

RAM needed to perform a fifty-minutes simulation, is 8 GigaBytes.

- OpenFOAM [28]: this is an open source software developed by the SGI corporation [29]. It is designed specifically to solve fluid dynamic problems. Like COMSOL, it implements several algorithms to solve PDEs and provides a large number of solvers, suitable for several computational fluid dynamic problems. It supports several external pre- and post-processing tools. This makes it very flexible.
  Since it is an open source software, the final users can customize the existing packages or create a new one according to their personal needs. The input data describing the geometry and the physical settings of the problem to be solved are given as a text file. On the one hand, this makes it easier to configure a set of configurations to be solved; on the other hand, the absence of a GUI makes the work of the user more complex.

CHAPTER

THREE

NLOC CONCEPT AND ARCHITECTURE

In this chapter we present a framework for *Networked Lab-on-Chip* (NLoC). More specifically, we will discuss the minimal set of functions that must be implemented by a NLoC and a system architecture that can support them. For each function we will provide alternative approaches that will be analyzed taking into account the design goals listed below:

- **Simplicity**: Proposed solutions have to be as simple as possible to guarantee reduced design costs.

- **Reliability**: Proposed solutions have to guarantee that the receiving NLoC element is able to recover the information sent by the transmitting NLoC element with controllable error probability

- **Capacity**: Proposed solutions have to support information transfer rates acceptable for the typical applications that will exploit NLoC.

- **Flexibility**: Proposed solutions have to be usable by the largest possible set of NLoC elements regardless of their specific characteristics and application objectives.

- **Energy efficiency**: Proposed solutions should minimize energy consumption in order to guarantee lower heating and – if battery-powered – longer battery duration.

Accordingly, in the rest of this chapter, we will first provide an overview of the NLoC concept and introduce the required notation in Section 3.1. Then, in Section 3.2 we will discuss the functions that are needed in NLoC systems and finally, in Section 3.3 we will propose an architecture which can support such functions.

3.1 Concept and notation

Current microfluidic systems consist of several specialized *elements* that are able to perform very specific operations, such as detection of a certain element in a sample or chemical operations over molecules. An example of such a system is the device depicted in Figure 3.1, on which a channel composed of three elements is shown: the first one is for the generation of a sample and of a reagent in form of droplets; the second one is a serpentine with very narrow spires for mixing the two droplets; the third part is a larger serpentine, which serves just as an extension of the channel: this is since an evental reaction needs a certain time to occur, before exiting the device. The circles represent the holes by which liquids are injected and expelled into/out from the chip. Typical microfluidic devices can contain tenths of these kind of elements, thus resulting in much more complex design.

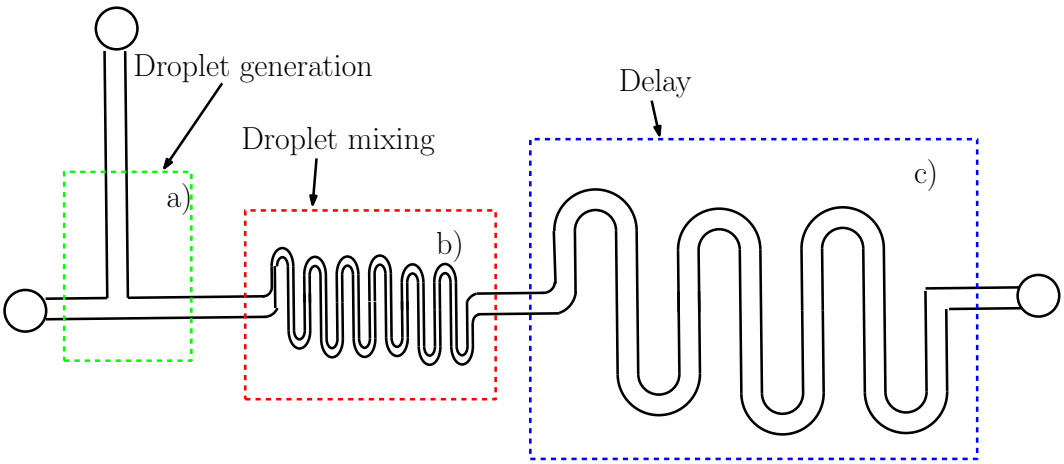

Figure 3.1: A simple microfluidic device, made of a) a component which generates droplet; b) a sequence of narrow spires in which droplets are mixed; c)a sequence of wider spires, to introduce a delay which allows reactions happen

Now, let us consider a microfluidic system Σ that includes a certain number M of elements denoted as $E_1^{(\Sigma)}, E_2^{(\Sigma)}, ..., E_M^{(\Sigma)}$, respectively. We denote as $f(E_i^{(\Sigma)})$ the function performed by $E_i^{(\Sigma)}$ and as $E^{(\Sigma)}(f)$ the element in Σ performing function f. An application, in its simplest form, requires a sequence of N functions to be performed. Let Φ denote an application and let $f_1^{(\Phi)}, f_2^{(\Phi)}, ..., f_N^{(\Phi)}$ represent the sequence of functions it requires.
Accordingly, samples of application Φ must traverse the sequence of elements $E^{(\Sigma)}(f_1^{(\Phi)}), E^{(\Sigma)}(f_2^{(\Phi)}), ..., E^{(\Sigma)}(f_N^{(\Phi)})$ where the output of an element should be given as input to another element. Currently, transportation from the output of an element to the input of another is performed:

- by manually moving the sample: this of course makes the system much more sensitive to human errors (spreading samples in the laboratory, damaging devices or equipment); moreover it requires time that could be saved by using an automatic control.

- by deploying appropriate dedicated pipes that connect the sequence of elements that will be traversed by the samples: this can significantly increase the complexity into the design of the device; for instance, in some cases it is necessary to develop devices in which channels are connected in three dimensional directions.

We propose to use networking technologies to perform such operation. More specifically, similarly to what is done in the Networks on Chip (NoC) domain [30], we assume that a networking element – that we call *microfluidic network interface* (MNI) – is attached to each element $E_i^{(\Sigma)}$ to perform the operations required for efficient, flexible and reliable exchange of samples with the other elements. We call *Networked Lab-on-a-Chip* (NLoC) the resulting system. Addressing functionality will be needed to make the MNIs communicate as detailed in the next sections.

3.2 NLoC functions

The objective of this section is to identify and discuss the minimal set of functions required by NLoC assuming that simplicity is the major design goal.

We will begin by focusing on the **transmission technique** that should be employed. Here two approaches are possible: *synchronous* and *asynchronous* transmissions. The first approach requires synchronization among all MNIs and this will affect requirements such as simplicity, reliability, energy; for this reason, asynchronous transmission is to be used in the proposed framework. This, however, requires the definition of a data structure, i.e., the packet. In NLoC – such as in traditional networking environments – the packet is divided into a *header* which contains information needed for performing networking operations and a *payload*. The header is a sequence of droplets which encodes the required service and/or the address of the element which should provide such service. Instead the payload may be a droplet containing the sample which is the object of the chemical/biomedical process performed by the LoC or a sequence of droplets encoding information exchanged by the elements of the NLoC.

Important issues to be considered are related to **addressing** and **routing**. The latter in particular is closely coupled with the logical topology which will be utilized and the type of interactions that the NLoC should support. In the near future it will be more convenient to concentrate the "intelligence" of the NLoC in a single element. Accordingly, the most appropriate model of interaction is of type *request/response* in which the central intelligence, which we call *microfluidic processing unit* (MPU) requests to a given element that an operation is performed on a sample. When such operation is completed, the element will respond by sending back the processed sample along with a report on whether the operation was correctly carried out or not. The MPU

according to the programmed job scheduling, will route the received sample to another element requesting the next operation, if any. It follows that the most appropriate *logical* topology to impose to the NLoC is a *star topology*. This simplifies the routing in the MNI significantly. In fact, all packets are generated by the MNI and should be delivered to the central hub (i.e. the intelligence).

Another important advantage of using such approach is that it does not require routing to be performed in the MNIs of the NLoC elements. Routing/switching will be performed by the central hub only. These aspects will be clarified in the following.

Finally, note that the above approach simplifies the **medium access control** (MAC) which might exploit a polling strategy. Polling however has low efficiency and therefore, we believe that in the future more efficient MAC schemes should be considered.

3.3 System architecture

In this section we will identify an architectural approach which fits with the design guidelines identified in the previous section. Starting from the logical star topology introduced in the previous section, as far as we want to maintain the capability of the NLoC to exchange droplets among LoC elements, the physical implementation of the star topology requires that the switching facilities of the system as a whole are concentrated into an MPU. However, use of an hydrodynamic switching matrix at the MPU would result in a prohibitive complexity and cost. So, alternative solutions should be implemented.

In the NoC literature all networking elements – named *routers* – have the same functionalities and are connected according to a grid topology [30] as

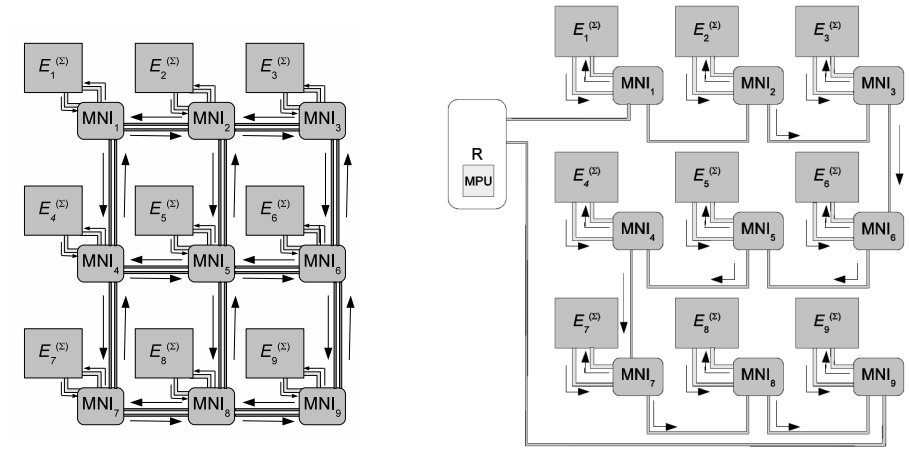

(a) (b)

Figure 3.2: Possible NLoC system architectures a) Grid topology, b) Ring topology.

shown in Figure 3.2a. This is not the most convenient solution for NLoCs, at least not at this time, for the following reasons:

- The grid topology requires each network element to be connected to its four neighbors by two directed channels. Realization of the micropumps required to operate all channels may cause a dramatic increase in cost and reduce the possibility of downscaling and integrating all the system.
- Hydrodynamic routers are complex systems and therefore replicating them many times could increase the overall complexity of the NLoC and, thus, again the cost.

Accordingly, we propose to use the architecture shown in Figure 3.2b,

where MNIs are connected through a ring. A router R, including also the MPU functionalities discussed in the previous section, is connected to the same ring and it is either the destination of the information generated by the MNIs or the source of all packets directed to the MNIs. Accordingly, the logical topology of the NLoC network is a star – as required in Section 3.2 – even if the physical topology is a ring.

Use of a ring topology allows to maintain the operations run by the MNIs extremely simple. In fact, the MNIs simply need to distinguish packets directed to them and forward them accordingly. Furthermore, they must perform a medium access control (which might be extremely simple and based only on polling operated by the router). Finally, they will have to generate packets which will reach the router R.

Comparing the two types of topology, it can be shown that the overall length of the pipes in the grid case is higher than in the ring case. This impacts the energy efficiency since longer pipes require higher pressure to be applied at the ends of the pipes and, therefore, higher energy costs. In fact, note that in the grid topology case, the overall length of the pipes is approximately

$$l_{\text{Grid}} \approx 4m(m-1) \tag{3.1}$$

where we assume that the M NLoC elements are located in a $m \times m$ grid (obviously $M = m^2$). Instead, in the case of ring topology, it can be demonstrated that the overall pipe length is approximately

$$l_{\text{Ring}} \approx \begin{cases} (2m^2+2m-4) & \text{if } m \text{ is even.} \\ (2m^2+4m-6) & \text{if } m \text{ is odd.} \end{cases} \tag{3.2}$$

By comparing the overall pipe lengths given in eqs. (3.1) and (3.2) we note that $l_{\text{Grid}} > l_{\text{Ring}}$ for all significant values of m.

Finally, observe that in the architecture shown in Figures 3.2 the router *R* incorporates the MPU functionalities discussed in the previous sections, i.e. it is the element which is able to perform processing [31] and can be *programmed* in order to implement the logic of complex applications over the NLoC platform. According to the proposed approach, the router *R* is the only manager of complex tasks. Again this fits with the guidelines provided in Section 3.2.

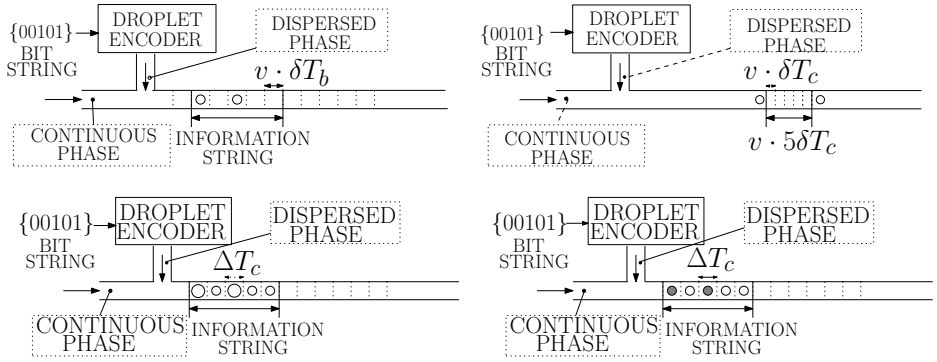

Figure 3.3: Droplet encoding a) Presence/absence of droplets b) Distance between droplets c) Size of droplets d) Substance composing droplets.

CHAPTER

FOUR

INFORMATION REPRESENTATION

In the previous chapters we discussed about the system topology to be considered in an NLoC. However to let the system properly work, we should be able to address the different LoC elements. Accordingly, we need to encode at least the information related to the address of the various elements without disregarding in any case the possibility to encode other information.

So, in this chapter we investigate on the droplet information encoding in microfluidic systems. More specifically, first we will describe different approaches that can be used to represent information. Then, the most promising of such approaches will be analyzed and compared.

4.1 Approaches

It is possible to encode information using different methodologies as discussed in the following:

- **Presence/absence of droplets**: This is the most obvious way of encoding information. Suppose that a string of n_b bits, $\{b_1, b_2, ..., b_{n_b}\}$ must be encoded. Suppose that the string is transmitted at time t_0. The encoder divides the interval $(t_0, t_0 + n_b \cdot \Delta T_b)$ in n_b time slots of duration ΔT_b each and generates a new droplet during the i-th slot if $b_i = 1$, while does not generate any new droplet if $b_i = 0$. For example, in Figure 4.1a we show the behavior of the encoder when we assume that the string to be transmitted is $\{00101\}$. Note that the receiver must implement the appropriate set of functionalities required to decode the information received through a train of droplets. If such methodology is employed, errors occur if different droplets belonging to the same train suffer different delays in the microfluidic channel and the receiver misinterprets the time slot where a certain droplet is located. Obviously, the larger is ΔT_b, the lower is the probability that errors occur; however, large values of ΔT_b cause low information rates. The selection of the most convenient value of ΔT_b requires availability of detailed channel models and knowledge of the interactions between the channel and the operations performed by the receiver. However these models are not available so far and therefore, call for basic research in the area of microfluidic system characterization and modeling.

- **Distance between consecutive droplets**: In this case several information bits are encoded in the distance between consecutive droplets. More specifically the string $\{b_1, b_2, ..., b_{n_b}\}$ is mapped to an integer value X. Then the encoder generates two droplets: one is transmitted immediately, the other after a time interval equal to $X \cdot \Delta T_c$.[1] As an

[1] Observe that as compared to the case when information is coded in the presence/absence of droplets, in this case $\Delta T_c < \Delta T_b$ because ΔT_b is lowerbounded by the need to avoid

example, in Figure 4.1b we show the behavior of the encoder assuming that the string to be transmitted is $\{00101\}$ again, and that the value of X corresponding to such string is $X = 5$. Also in this case errors occur if the two droplets are subject to different delay and therefore the receiver achieves a wrong estimation of X. Obviously, in this case the larger is ΔT_c, the lower the probability that estimation of X is erroneous; however, large values of ΔT_c cause low information rate. Accordingly, as discussed in case of information encoding based on the presence/absence of droplets, appropriate channel models are required.

- **Size of the droplets**: In this case coding exploits the capability of generating (and then distinguishing) droplets with different size. As an example, we can consider the case in which droplets can be generated and distinguished based on two different sizes. Small droplets are used to represent '0's whereas large droplets are used to represent '1's. Such methodology can be considered as a generalization of the "Presence/absence of droplets" methodology (in that case the size of small droplets was zero, i.e., absence of the droplet). In Figure 3.3c, we show the behavior of the encoder when the string to be represented is the usual one, i.e., $\{00101\}$. It follows that errors can occur due to the same reasoning discussed above. Furthermore, while traversing the microfluidic channel, droplets will be subject to deformations which may also cause errors at the receiver. Obviously the probability of such errors decreases when the difference in the size of the droplets increases.

  Finally, note that the information rate can be increased by considering several droplet sizes to encode symbols representing several bits. As an example, we can encode symbols representing two bits by generating

interactions between consecutive droplets.

droplets with four different sizes. This increase in the encoding rate is however masked by larger probability of errors because distinguishing between several droplet sizes may be an operation more prone to errors.

- **Substance composing the droplets**: Information is encoded in the substance composing the droplets. Implementation of transmitters which perform such encoding policy is very simple, because different pumps are used, which is a clear advantage. At the receiver, solutions are required which are able to distinguish droplets made of different substances which involves significant complexity. In Figure 3.3d, we show the behavior of the encoder when the string to be represented is again $\{00101\}$. In this case errors are caused by wrong processing operations on the droplets at the receiver. Observe that the probability of such errors decreases as the difference in the physical parameters and characteristics of the substances utilized to encode bits increases. However, as such difference increases, the behavior of the corresponding droplets in the microfluidic channel becomes much different and sometimes unpredictable.

Accurate regulation of the droplet size at the transmitter or analysis of the substances composing the droplets at the receiver are extremely complex and costly operations with current technologies; so it can be expected that the first generation of NLoCs will employ information encoding schemes based on the presence/absence of droplets or on the distance between consecutive droplets. Furthermore, choice between these two encoding schemes impacts on the design of the microfluidic network devices and, consequently, on the manufacturing process and cost. In fact, presence/absence of droplets encoding requests a strict droplet synchronization as compared to the distance encoding; so we believe that in the next future the best way to encode infor-

mation is to use the distance D_{Enc} between consecutive droplets.

Nevertheless, since microfluidic computing devices have been already designed which use the presence/absence of droplets (e.g., [22]), in the following we will compare their channel capacity with what can be obtained by using droplet distance encoding and characterize the propagation for some physical set-ups.

The transmission capacity for an encoding scheme using the presence/absence of droplets is given by:

$$C_{PA} = v/\Delta \tag{4.1}$$

where v is the velocity of the droplets (in m/s) and Δ is the distance (in m) between two consecutive droplets. It can be shown that in case of distance encoding the capacity C_{DD} can be approximated using the relationship between the mutual information and the entropy (conditioned or not) [32] as

$$C_{DD} = \frac{v}{S/2+\Delta} \log_2 \left(\frac{S}{\sqrt{2\pi e}\sigma_E} \right) \tag{4.2}$$

where e is the Napier's constant, σ_E is the standard deviation of the error and Δ is again the variable representing distance between consecutive droplets. This is an equation in the parameter S: the latter is the maximum value within which distance between consecutive droplets can be choosen in such a way that they do not interact. Let $S_{\max}$ be the value of S which maximizes eq. (4.2).

4.2 Channel capacity

The encoding of information in droplet microfluidic systems can be performed in different ways. Some possible mechanisms are presence/absence

of droplets, distance between consecutive droplets, size of droplets, substance composing droplets. However, accurate regulation of the droplet size at the transmitter or analysis of the substances composing the droplets at the receiver are extremely complex and costly operations with current technologies. Thus, the first generation of HCNs will likely employ information encoding schemes based either on the presence/absence of droplets or on the distance between consecutive droplets.

To this purpose, in Figure 4.1 we show how a string of bits, for example ”00101”, can be encoded in HCNs. More specifically, in Figure 4.1(a) presence/absence encoding is illustrated: a bit ”1” is encoded into presence of a droplet and a bit “0” is encoded into absence of a droplet. In Figure 4.1(b), instead, the bit string is converted into a number, e.g., the string $00101 = 5$, and the droplet encoder generates two droplets which are distant 5δ from each other, where δ represents the granularity supported by the HCN and depends on the noise introduced by the microfluidic channel and the precision of the receiver. Observe that, the choice between these two encoding schemes impacts on the design of the microfluidic network devices and, consequently, on the manufacturing process and cost. In fact, encoding based on the presence/absence of droplets requires a strict droplet synchronization as compared to distance encoding; accordingly for worth of simplicity, in this paper we will focus on the case of information encoded in the distance D_{Enc} between consecutive droplets. In the rest of this section, we will calculate the maximum information rate, C_{DD}, that can flow through a microfluidic channel. To this purpose, we will exploit two experimental evidences we have observed in our tests:

1. **Experimental evidence 1:** droplets interact with each others when their distance is below a given threshold Δ which depends on a large

number of physical factors. Such interactions usually result in droplets coalescence (i.e. fusion) which may cause errors. If the distance between droplets is higher than Δ, droplets do not interact with each other [33].

2. **Experimental evidence 2:** given two consecutive droplets, their distance at the receiver, D_{Dec}, is different from their distance at the transmitter, D_{Enc}. The difference between the above distances, $E = D_{\text{Dec}} - D_{\text{Enc}}$, can be regarded as an additive noise in the proposed system. In Section 4.3 we will show that E can be modeled as a Gaussian random variable characterized by an average value 0 and a variance σ_E^2 (see Figure 4.7). Moreover such noise does not depend on the observed point in the micro-channel as illustrated in Figure 4.6.

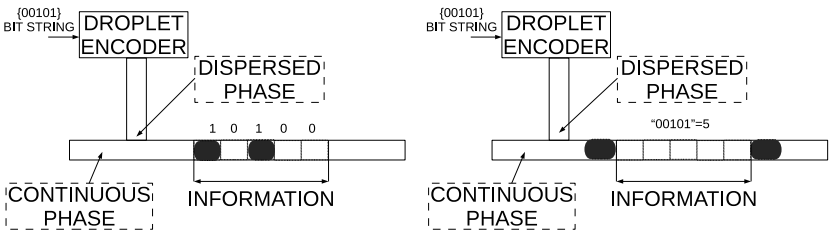

Figure 4.1: Droplet encoding a) Presence/absence of droplets b) Distance between droplets.

The maximum information rate, C_{DD}, can be written as:

$$C_{DD} = \max_{T_S} \left(\frac{C_S}{T_S} \right), \tag{4.3}$$

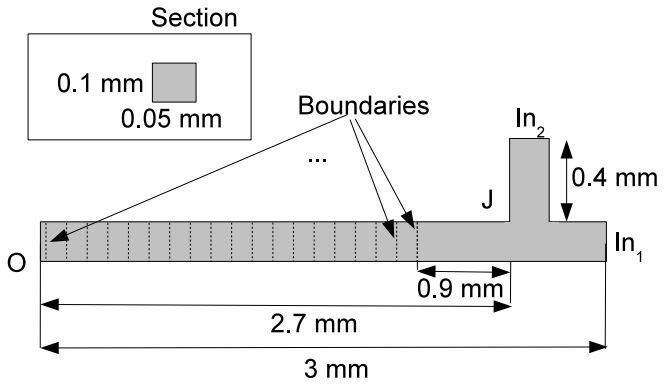

Figure 4.2: Setup for the simulation of the T-Junction.

where C_S represents the capacity for each channel use when the average time interval between two consecutive channel uses is equal to T_S. As a consequence of Experimental evidence 1, the average time interval between two channel uses must be larger than Δ/v to avoid coalescence, where v is the average velocity of droplets moving in the microfluidic channel. Accordingly, we write T_S as

$$T_S = \frac{\Delta + S}{v}, \tag{4.4}$$

where S is a positive value. Therefore, (4.3) can be rewritten as follows

$$C_{DD} = \max_{T_S} \frac{v \cdot C_S}{\Delta + S}. \tag{4.5}$$

In the following, we will first demonstrate that C_S can be calculated as:

$$C_S = \log_2 \left(\frac{eS}{\sqrt{2\pi e \sigma_E^2}} \right), \tag{4.6}$$

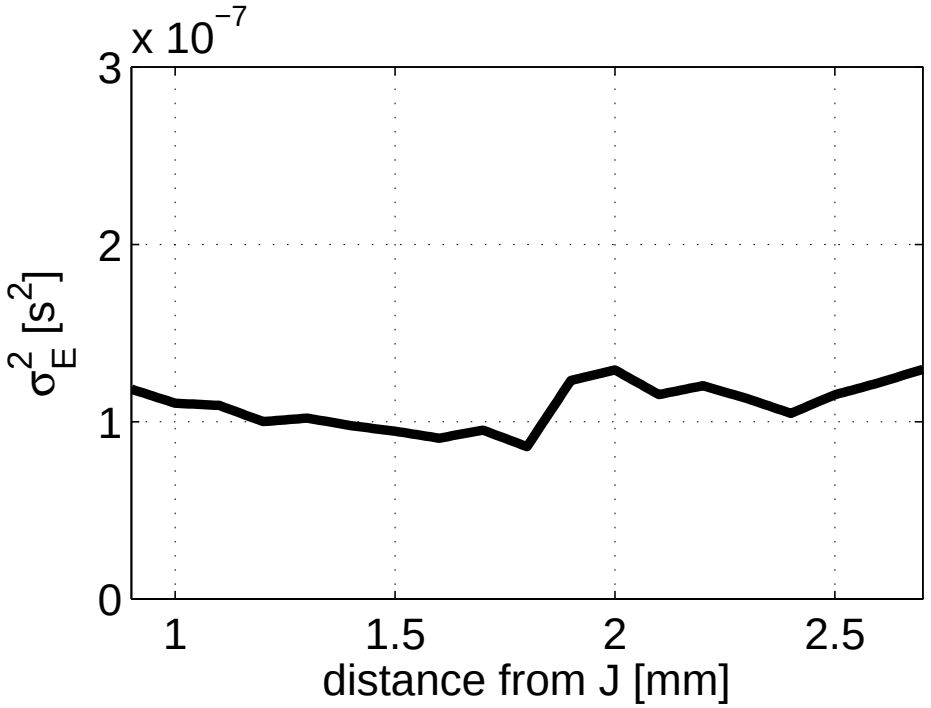

Figure 4.3: Variance of the error σ_E^2 divided by the square of the droplets velocity v^2 at different boundaries of the T-junction assuming $\eta_r = 3.441$.

where σ_E^2 is the variance of the noise E as mentioned above.

Then, we will use (4.6) to demonstrate that C_{DD} is given by:

$$C_{DD} = \frac{v}{\sqrt{2\pi e \sigma_E^2} \log 2} e^{-W\left(\frac{\Delta}{\sqrt{2\pi e \sigma_E^2}}\right)}, \tag{4.7}$$

where $W(\cdot)$ is the Lambert W function and is defined through the inverse relationship

$$z = W(z) e^{W(z)}. \tag{4.8}$$

Let us start by proving (4.6). First, note that the average time interval between two channel uses is equal to the average time interval between the generation of two consecutive droplets. This can be calculated as the average distance between two consecutive generated droplets, $E\{D_{\text{Enc}}\}$, divided by the average velocity v. Accordingly, we can calculate T_S as

$$T_S = \frac{E\{D_{\text{Enc}}\}}{v}. \tag{4.9}$$

To avoid coalescence, the distance between droplets set by the transmitter, D_{Enc}, must be larger than Δ. Accordingly, we write D_{Enc} as:

$$D_{\text{Enc}} = \Delta + X, \tag{4.10}$$

where X represents a positive random variable with average value equal to S, i.e. $\eta_X = S$.

It follows that the capacity C_S can be written as a function of the mutual information between the distance of two consecutive droplets at the transmitter and at the receiver, i.e. $I(D_{\text{Dec}}, D_{\text{Enc}})$. More specifically, C_S is given by [32]:

aas

$$\begin{aligned} C_S &= \max_{f_X(x):\eta_X=S} I(D_{\text{Dec}}, D_{\text{Enc}}) = \\ &= \max_{f_X(x):\eta_X=S} [h(D_{\text{Dec}}) - h(D_{\text{Dec}}|D_{\text{Enc}})] = \\ &= \max_{f_X(x):\eta_X=S} [h(D_{\text{Dec}}) - \\ &\quad -h(D_{\text{Enc}} + E|D_{\text{Enc}})] = \\ &= \max_{f_X(x):\eta_X=S} [h(D_{\text{Dec}}) - h(E|D_{\text{Enc}})], \end{aligned} \tag{4.11}$$

where $h(\cdot)$ is the differential entropy. By assuming that the noise E is independent of the distance between the droplets, it follows that $h(E|D_{\text{Enc}}) = h(E)$. Furthermore, given that the noise E is Gaussian, its differential entropy is given by

$$h(E) = \log_2(\sqrt{2\pi e}\sigma_E). \tag{4.12}$$

It follows that (4.11) can be rewritten as

$$C_S = \max_{f_X(x):\eta_X=S} [h(D_{\text{Dec}})] - \log_2(\sqrt{2\pi e}\sigma_E). \tag{4.13}$$

Given that the error is Gaussian with average value equal to 0, the average value of the distance between two droplets at the transmitter and at the receiver is the same. Moreover, if we suppose that the probability that such distance is lower than Δ is negligible as in [34], we observe that $\max_{f_X(x):\eta_X=S}[h(D_{\text{Dec}})]$ is equal to the entropy of an exponential variable (i.e. the one which maximizes the differential entropy) with average equal to S, that is

$$\max_{f_X(x):\eta_X=S} [h(D_{\text{Dec}})] = \frac{1 - \log(1/S)}{\log(2)} = \log_2(e \cdot S). \tag{4.14}$$

By replacing (4.14) in (4.13) we obtain

$$\begin{aligned} C_S &= \log_2(e \cdot S) - \log_2(\sqrt{2\pi e}\sigma_E) = \\ &= \log_2\left(\frac{e \cdot S}{\sqrt{2\pi e \sigma_E^2}}\right), \end{aligned} \tag{4.15}$$

which proves (4.6).

Eq. (4.6) can be used to demonstrate (4.7). To this purpose, let us plug (4.6) in (4.5). Accordingly, we obtain:

$$C_{DD} = \max_{S>0} \frac{v \cdot \log_2 \left(\frac{eS}{\sqrt{2\pi e \sigma_E^2}} \right)}{\Delta + S}. \tag{4.16}$$

In order to find the maximum value required in (4.16) we need to evaluate the derivative of $\frac{\log_2 \left(\frac{eS}{\sqrt{2\pi e \sigma_E^2}} \right)}{\Delta+S}$ with respect to S. Then, we must find the values of S for which such derivative is equal to 0. Accordingly, we have to calculate the values of S such that

$$\begin{aligned} &\Delta + S - S\log \left(\tfrac{\sqrt{e}S}{\sqrt{2\pi}\sigma_E} \right) = 0 \Rightarrow \\ &S \left(\log \left(\tfrac{\sqrt{e}S}{\sqrt{2\pi}\sigma_E} \right) - \log e \right) = \Delta \Rightarrow \\ &S\log \left(\tfrac{S}{\sqrt{2\pi e}\sigma_E} \right) = \Delta \Rightarrow \\ &\tfrac{S}{\sqrt{2\pi e}\sigma_E} \log \left(\tfrac{S}{\sqrt{2\pi e}\sigma_E} \right) = \tfrac{\Delta}{\sqrt{2\pi e}\sigma_E}. \end{aligned} \tag{4.17}$$

By denoting $B = \left(\log \frac{S}{\sqrt{2\pi e}\sigma_E} \right)$ it follows that

$$Be^B = \frac{\Delta}{\sqrt{2\pi e}\sigma_E}. \tag{4.18}$$

Therefore

$$B = \left(\log \frac{S}{\sqrt{2\pi e}\sigma_E} \right) = W \left(\frac{\Delta}{\sqrt{2\pi e}\sigma_E} \right), \tag{4.19}$$

where $W(\cdot)$ is the above mentioned Lamber W function. Accordingly, there is only one value of S which satisfies (4.17), that is

$$S^* = \sqrt{2\pi e}\sigma_E e^{W\left(\Delta/(\sqrt{2\pi e}\sigma_E)\right)}. \tag{4.20}$$

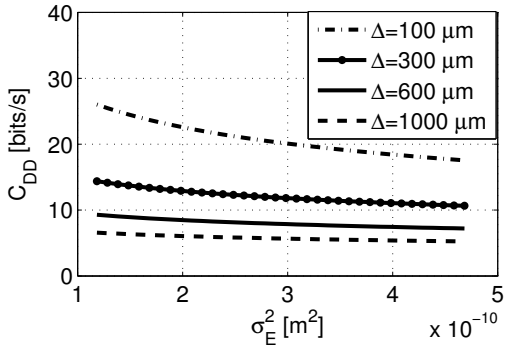

Figure 4.4: C_{DD} as a function of the variance of the noise, σ_E^2, for different values of Δ when $v = 2mm/s$.

It is possible to prove that the second derivative of $\frac{\log_2\left(\frac{eS}{\sqrt{2\pi e\sigma_E^2}}\right)}{\Delta+S}$ with respect to S is lower than 0 when $S = S^*$. So S^* is the searched maximum value. Finally, by plugging (4.20) in (4.16) we obtain the expression in (4.7) which concludes our demonstration.

In Figure 4.4 we show the impact of the variance of the noise, σ_E^2, and the threshold Δ on the capacity C_{DD}. As expected,

- an increase in σ_E^2 decreases system performance in terms of maximum information rate.

- an increase in Δ, that is the minimum droplets' distance to avoid coalescence, results in a decrease in C_{DD}.

$$\frac{\Delta}{\sigma_E} > \frac{e\sqrt{2\pi e}\ln 2\, e^{1/\ln 2}}{2} = 16.4772 \tag{4.21}$$

In [12] and [13] we have evaluated the value of the ratio Δ/σ_E as a function of several design parameters, such as

- η_r, representing the ratio between the viscosity of the continuous phase η_c and the viscosity of the dispersed phase η_c, i.e. $\eta_r = \eta_c/\eta_d$. The corresponding curve is represented in Figure 4.10. In particular, it has been choosen $\eta_c = 6.71 \cdot 10^{-3}$ Pa $\cdot$ s and $\eta_d \in [1.95 \cdot 10^{-3}, 6.71 \cdot 10^{-3}]$ Pa $\cdot$ s.

- Q_C, that is the flowrate at which the continuous phase is injected into the pipe. To this purpose we represent two curves in Figure 4.11: one was obtained when the distance from the injection point is $d = 0.6$ mm and the other when $d = 2.7$ mm.

4.3 Channel characterization

In this section we characterize the noise statistics in the microfluidic channel relevant to information encoding/decoding for different values of the viscosity of the fluids. To this goal, we have run a large set of simulations aimed at the characterization of how droplets flow in microfluidic channels. We have used the OpenFOAM simulator [28] to investigate the standard microfluidic configuration shown in Figure 4.2 and usually denoted as *T-junction*.

In this configuration there are two inlets (where fluids enter the system), In_1 and In_2, and an outlet O. The continuous phase, that is the fluid which carries the droplets, enters from inlet In_1 while the dispersed phase, i.e., the fluid which composes the droplets, enters from In_2. Sections of all Pipes are 0.1×0.05 mm^2 in size. We assume that the viscosity of the dispersed phase is $6.71 \cdot 10^{-3}$ Pa $\cdot$ sec, whereas the viscosity of the continuous phase can assume a value in the range $[1.75 \cdot 10^{-3}, 7.8 \cdot 10^{-3}]$ Pa $\cdot$ sec.

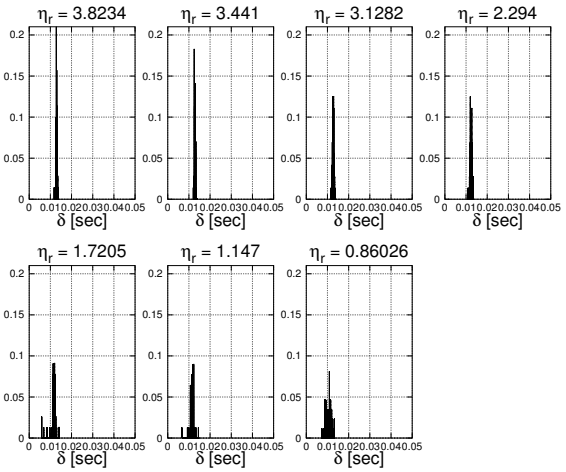

Figure 4.5: Probability density functions of time interval between successive droplets evaluated at boundary 10 for several values of η_r (in decreasing order).

The dispersed phase entering from inlet In_2 forms droplets at the intersection point junction J at a constant rate. These droplets will be transported by the continuous phase throughout the channel to the outlet O. The distance between the point J and the outlet O is equal to 2.7 mm. We considered 19 observation points (called *boundaries*) equally spaced along the branch $J-O$. In our experiments we measured the interarrival time between pairs of consecutive droplets at such boundaries, for different values of the ratio η_r between the viscosities of the dispersed and continuous phases.

For example, in Figure 4.5 we show the probability density functions of the interarrival time between consecutive droplets at boundary 10, for different values of the ratio η_r between the viscosity of the dispersed and the continuous phase. In Figure 4.5 we observe that the variance of the droplet inter-arrival time increases as the viscosity of the continuous phase increases and, thus, η_r decreases.

This is because when the viscosities of the two fluids differ, they tend to exhibit resistance in motion which leads to a larger variance in the inter-arrival time between consecutive droplets.

As discussed in Section 4.3, the performance of the encoding scheme depends on the values of both Δ and the variance of the error. As far as Δ is concerned, this does not depend on the boundary where we observe the flux of droplets. On the contrary, we would expect that the variance increases as the distance between the considered boundary and the intersection point J increases, as in traditional communication systems where the signal quality decreases as it propagates through the channel.

Accordingly, in Figure 4.6 we show the value of the variance of the error E observed at different distances from the intersection J. Variations of the values reported in figure, which has been obtained by considering 100 observations, are due to a large number of factors such as pressure fluctuations

(which occur especially in the proximity of the junction) and imperfections and roughness in the microfluidic channel (which are modeled in OpenFoam through appropriate setting of simulation parameters). Deep investigation of the above phenomena is the subject of current chemical and physical research, see for example [35, 36], and is beyond the scope of this paper. Here we note however that, surprisingly, the variance does not increase in a noticeable way as the distance from the intersection J increases.

This means that, in microfluidic communication channels, the quality of the signal does not decrease as the distance between the sender and the receiver increases. In Figure 4.7, we represent the cumulative distribution function of the error E measured at the intersection distant 1.4 mm from J. Let us notice that the cumulative distribution function of E, $F_E(e)$, obtained in our simulations fits perfectly the cumulative distribution function of a Gaussian random variable. This is expected given that E derives from the interactions between a huge number of particles.

In Figure 4.8, we show the value of Δ/v vs. the ratio η_r. In this figure we observe that the value of Δ/v increases as the above ratio η_r increases and, thus, the information capacity of the encoding scheme is expected to worsen. Finally, in Figure 4.9 we show the value of the standard deviation of the error (i.e. the noise), σ_E, divided by the velocity v, versus the ratio η_r. When the ratio η_r increases, σ_E/v decreases and therefore, the information capacity increases.

4.3.1 Characterization of distance between consecutive droplets

In the next chapter we present an example of design of a reliable pure hydrodynamic switch able to manage the information about the destination address

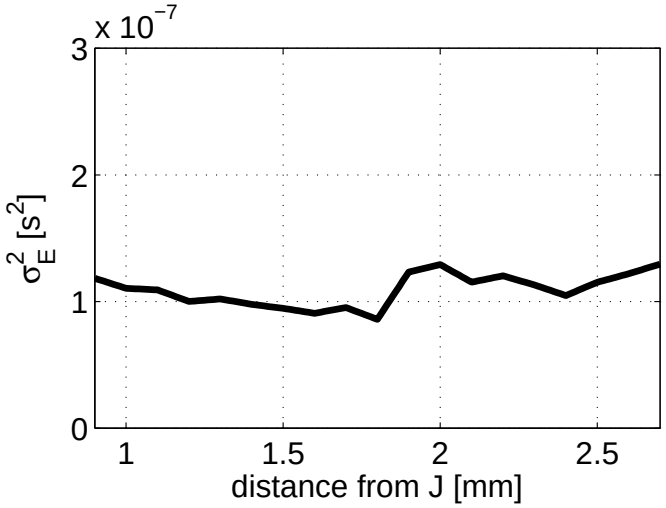

Figure 4.6: Variance of the error σ_E^2 divided by the square of the droplets velocity v^2 at different boundaries of the T-junction assuming $\eta_r = 3.441$.

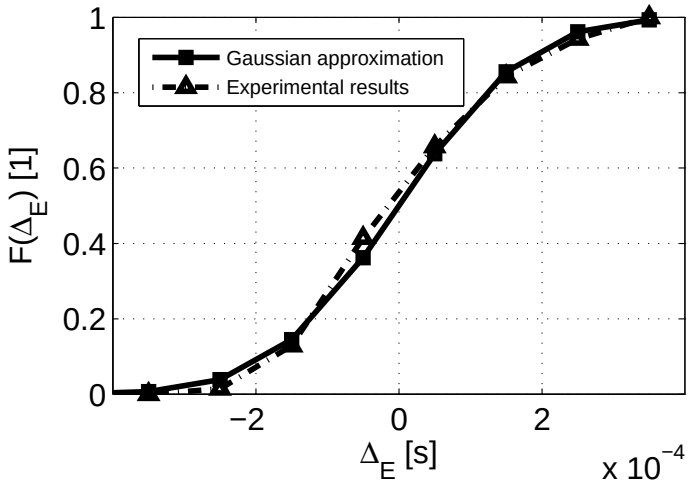

Figure 4.7: Cumulative distribution function $F_E(e)$ of the error E and its Gaussian approximation assuming $\eta_r = 3.441$.

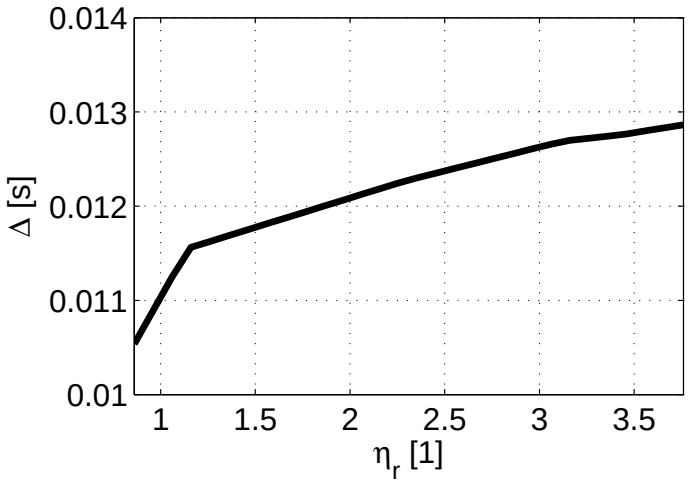

Figure 4.8: Values of Δ/v vs. the ratio η_r.

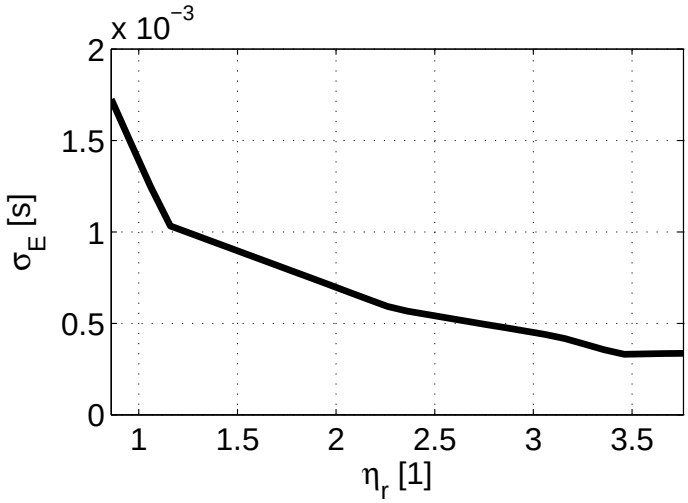

Figure 4.9: Values of σ_E/v vs. the ratio η_r.

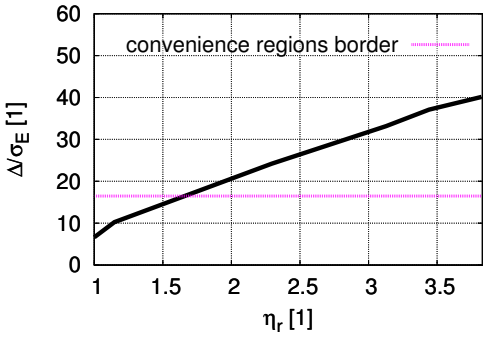

Figure 4.10: Values of the ratio Δ/σ_E vs. the ratio between the viscosity of the continuous and dispersed phases.

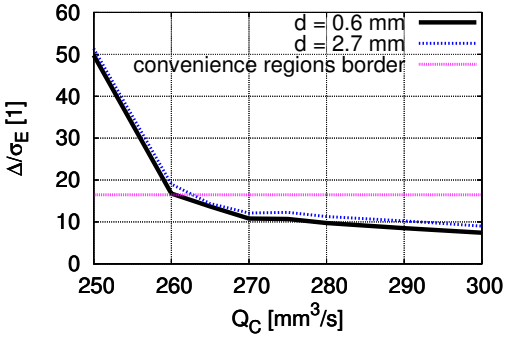

Figure 4.11: Values of the ratio Δ/σ_E vs. the flowrate of the continuous phase for two different values of the distance from the njection point.

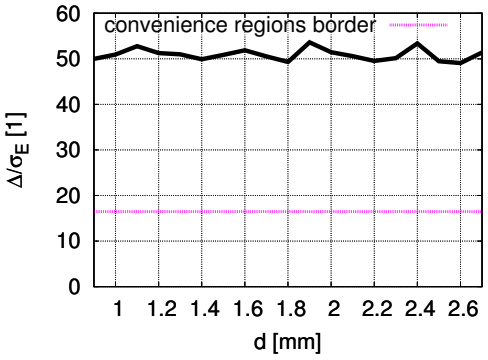

Figure 4.12: Values of the ratio Δ/σ_E vs. the distance from the injection point.

encoded as distance between droplets. This switch is the MNI illustrated in Figure 3.2b and its purpose is to forward the droplets containing the samples towards the microfluidic element attached to it or let them continue to flow towards the next MNI in the ring.

In this context, it is useful to statistically characterize the distance between droplets, D_{Dec}, at the receiving MNI.

By assumption that the noise E is additive and independent on the distance between droplets at the transmitter[2], D_{Enc}, thus we can calculate the probability density function of D_{Dec}, that is, $f_{D_{\text{Dec}}}(x)$ as given below:

$$f_{D_{\text{Dec}}}(x) = (f_{D_{\text{Enc}}} \star f_E)(x), \tag{4.22}$$

where $f_{D_{\text{Enc}}}(x)$ represents the probability density function of the distance between the droplets at the transmitter, $f_E(x)$ represents the probability density function of the noise, and '$\star$' represents the convolution product. By recalling that the noise is Gaussian, thus

$$f_E(t) = \frac{1}{\sqrt{2\pi\sigma_E^2}} e^{-\frac{t^2}{2\sigma_E^2}} \tag{4.23}$$

and assuming that D_{Enc} is uniformly distributed in the interval $[\Delta, \Delta + X_{\max}]$ (which guarantees a bound on the transmission delay), i.e.,

$$f_{\text{Enc}}(t) = \begin{cases} 1/X_{\max} & \Delta \leq t \leq \Delta + X_{\max} \\ 0 & \text{otherwise} \end{cases} \tag{4.24}$$

[2] This assumption is justified by the fact that, by assuming that such droplets distance is higher than Δ, as stated in experimental evidence1, droplets do not interact with each others.

we obtain

$$f_{D_{\text{Dec}}}(x) = \int_{-\infty}^{+\infty} f_{\text{Enc}}(t) f_E(-t+x)dt = \frac{1}{2 \cdot X_{\max}} \cdot \\ \cdot \left[\text{erf}\left(\frac{x-\Delta}{\sqrt{2}\sigma_E} \right) - \text{erf}\left(\frac{x-\Delta-X_{\max}}{\sqrt{2}\sigma_E} \right) \right]. \tag{4.25}$$

CHAPTER

FIVE

SWITCHING DROPLETS IN HYDRODYNAMICALLY CONTROLLED NETWORKS

In our approach we suppose that the samples which should be chemically treated or analyzed by the Hydrodynamically Controlled Networks HCN are included in a *payload droplet*. In order to route the payload droplet appropriately, our HCN switching scheme exploits another droplet, which is called *header droplet*, that is used for network signaling only and, in particular, for encoding the destination address. The *destination address* is encoded in the distance between the header droplet and the payload droplet. The HCN switching block of the i-th MNI consists of the T-junction circuit represented in Figure 5.1. This circuit has one inlet arriving from the previous MNI in the ring, that is the $(i-1)$-th MNI. The inlet is connected to a Pipe which bifurcates in B in two opposite Pipes denoted as Pipe 1 and Pipe 2.

The points at the end of Pipe 1 and Pipe 2, denoted as A and C, respec-

tively, are connected by a channel characterized by very low hydrodynamic resistance, which we call *bypass channel*. Then, Pipes 1 and 2 continue into Pipes 3 and 4, respectively.

At the end of Pipes 3 and 4 there are two outlets:

- the outlet out_i' at the end of Pipe 3 is connected to the i-th element, $E_i^{(\Sigma)}$.
- the outlet out_i'' at the end of Pipe 4 is connected to the inlet of the next MNI in the ring, i.e., it is connected to the input of the $(i+1)$-th MNI.

The bypass channel connecting A and C guarantees that the pressure at the above two points is equal [10]. Accordingly, the pressure difference between points B and A, which we denote as $\Delta P_i^{(BA)}$, is equal to the pressure difference between points B and C, which we denote as $\Delta P_i^{(BC)}$. This occurrence makes the droplet behavior in the MNI microfluidic circuit represented in Figure 5.1 dependent on the geometric characteristics of Pipe 1 and Pipe 2 only, as will be demonstrated in Section 5.1.

In the following, we derive the HCN design parameters which allow the MNI to decode the destination address and therefore to switch the payload droplet related to the microfluidic element attached to itself. More specifically, in Section 5.1 we will first identify the conditions in which the header droplet enters Pipe 2 at the bifurcation B. Then, in Section 5.2 we will identify the conditions in which the payload droplet enters Pipe 1 if its distance from the header droplet is such that the latter is still in Pipe 2, while enters Pipe 2 when the header droplet has already left Pipe 2:

- in the first case the payload arrives to the i-th element, $E_i^{(\Sigma)}$, whereas the header droplet will be forwarded by the MNIs until it reaches the μR that discards it;

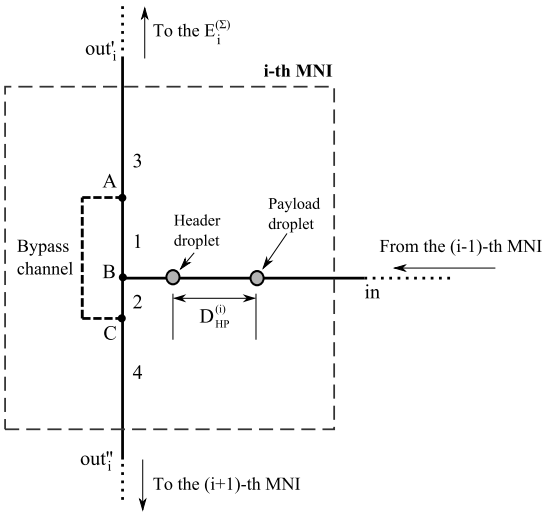

Figure 5.1: Distance-based switching.

- in the second case the payload droplet follows the header droplet in the ring, and arrives to the next MNI.

As a consequence, μR must guarantee that the distance between the header and the payload droplets is appropriate at each MNI. This is not a straightforward issue; in fact, the distance between the header droplet and the payload droplet is modified at each MNI as explained in Section 5.3.

Finally note that droplets must leave the MNI before next droplets can be switched; otherwise, prior droplets would interfere with the switching behavior.

5.1 Controlling the header droplet

We will study the microfluidic circuit shown in Figure 5.1 by exploiting the Hagen-Poiseuille's law $\Delta P = R_{\text{hyd}} Q$ where ΔP is the difference in pressure at the end points of a Pipe, R_{hyd} represents the hydrodynamic resistance of the Pipe, and Q is the flux in the Pipe. Accordingly, we need to solve the microfluidic circuit represented in Figure 5.2a.

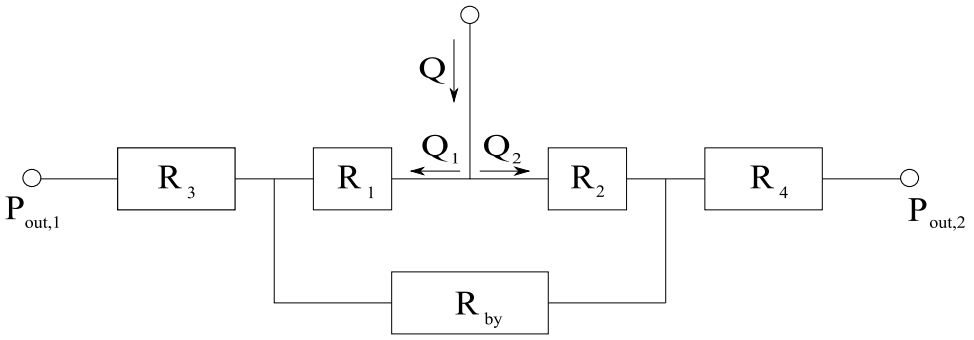

(a) Microfluidic equivalent circuit of the MNI

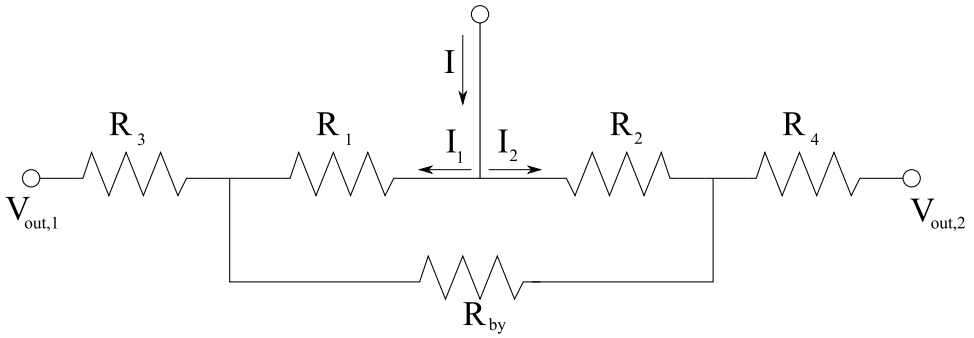

(b) Electrical equivalent circuit of the MNI

Figure 5.2: Equivalent microfluidic and electrical circuits for the MNI represented in Figure 5.1.

An analogy with the Ohm's law ($\Delta V = RI$) can be easily drawn [19]. Therefore we approach our design problem by using the electrical equivalent circuit shown in Figure 5.2b where the pressure difference ΔP is replaced by the voltage difference ΔV, and the flow rate Q is replaced by the electric current I. In both Figures 5.2a and 5.2b, note that:

- R_1 and R_2 represent the equivalent resistance of Pipe 1 and 2, respectively;
- R_3 represents the equivalent resistance at the end point of Pipe 1, A, towards the element $E^{(\Sigma)}$;
- R_4 represents the equivalent resistance at the end point of Pipe 2, C, towards the next MNI in the ring.

A droplet arriving at a bifurcation always enters the Pipe with higher flow rate [8, 20]. Therefore, to appropriately address the element $E^{(\Sigma)}$, initially we want to evaluate how to set the T-junction characteristics in such a way that $Q_2 > Q_1$ (or analogously $I_2 > I_1$) when the header droplet arrives at the bifurcation point.

By applying the Kirchhoff laws we have

$$\begin{cases} I = I_1 + I_2 \\ I_1 - I_{R_3} - I_{R_{by}} = 0 \\ I_2 + I_{R_{by}} - I_{R_4} = 0 \\ I_1 R_1 - I_2 R_2 + R_{by} I_{R_{by}} = 0 \\ V_{out,1} + V_{R_3} + R_1 I_1 - R_2 I_2 - V_{R_4} - V_{out,2} = 0. \end{cases} \tag{5.1}$$

By moving to the hydrodynamic domain, the solution of the system of

equations in (5.1) gives:

$$\frac{Q_1-Q_2}{Q}=\frac{1}{R_1+R_2+R_{by}}\left[\frac{(R_2-R_1)(R_3+R_4)}{(R_3+R_4)+R_{by}(R_1+R_2)}+\right.$$
$$+R_{by}\left(\frac{(R_2-R_1)+(R_4-R_3)}{(R_3+R_4)+R_{by}(R_1+R_2)}+\right. \tag{5.2}$$
$$\left.\left.+\frac{\frac{2}{Q}(P_{\text{out},2}-P_{\text{out},1})}{(R_3+R_4)+R_{by}(R_1+R_2)}\right)\right].$$

Usually, we can assume $P_{\text{out},2}\simeq P_{\text{out},1}$ since in the end all fluids will be collected in a sink at the atmospheric pressure. Furthermore, we realize the bypass channel with a very large width (when compared to other Pipes in the circuit) so that $R_{by}<<\min\{R_3,R_4\}$.

If the above conditions are satisfied, (5.2) can be rewritten as

$$\frac{Q_1-Q_2}{Q}\simeq\frac{R_2-R_1}{R_1+R_2+R_{by}}+\frac{R_{by}}{R_1+R_2+R_{by}}\frac{R_4-R_3}{R_4+R_3}. \tag{5.3}$$

Finally taking into account that usually R_3 and R_4 are very large when compared to the other hydrodynamic resistances involved in the circuit represented in Figure 5.2(b), we can further approximate (5.3) as follows

$$\frac{Q_1-Q_2}{Q}\simeq\frac{R_2-R_1}{R_1+R_2+R_{by}}. \tag{5.4}$$

By exploiting the condition in (5.4) the sign of Q_1-Q_2 will depend on the sign of R_2-R_1. Accordingly, if $R_2<R_1$ and thus $Q_2>Q_1$, then the header droplet enters Pipe 2 when arrives at the bifurcation point B, as desired.

In order to impose the relationship, $R_2<R_1$, we exploit the results of the theoretical framework in [19]. The hydrodynamic resistance, R, of a rectangular channel with length L, height h, and width w, traversed by a monophase

flow is given by

$$R = \frac{\Delta p}{Q} \simeq \frac{12\mu L}{h^3 w(1-0.63h/w)} = \alpha \frac{L}{w} \quad \text{with } h < w, \tag{5.5}$$

where μ denotes the fluid viscosity and α is defined as follows:

$$\alpha = \frac{12\mu}{h^3(1-0.63h/w)}. \tag{5.6}$$

Accordingly, in order to have $R_2 < R_1$, that is the header droplet enters Pipe 2 at the bifurcation point B, from (5.5) the length of Pipe 2 must be smaller than the length of Pipe 1:

$$L_2 < L_1. \tag{5.7}$$

5.2 Controlling the payload droplet

In order to appropriately control the direction taken by the payload droplet when it arrives to the bifurcation point B, we must impose that the presence of the header droplet in Pipe 2 inverts the sign of the difference between the hydrodynamic resistances of Pipes 2 and 1, respectively.

This is feasible because the presence of a droplet in Pipe 2 increases the hydrodynamic resistance of such Pipe. We denote the increased resistance as R_2'.

Although it is difficult to accurately predict the resistance added by a droplet in a Pipe, several studies confirm that the hydrodynamic resistance R' of a micro-channel with a rectangular section containing n droplets, can be approximated as [3, 37, 38]

$$R' = R(\eta_r \phi + 1 - \phi) + n\left[3.15 f(\eta_r)\frac{\sigma}{h} Ca^{2/3} \frac{1}{v \cdot w \cdot h}\right], \tag{5.8}$$

where

- R is the hydrodynamic resistance in case no droplets are currently in the micro-channel;
- Ca is the capillary number;
- $\phi = n \cdot L_D/L_C$ is the fraction of the micro-channel occupied by the droplets, where L_C and L_D represent the lengths of the channel and the droplet, respectively;
- $f(\eta_r)$ is a function of the viscosity ratio varying between 1 and about 1.5 when η_r spans from 0 to $+\infty$ [39];
- v is the velocity of the droplets;
- σ is the surface tension coefficient.

In the following we will find approximate expressions for the hydrodynamic resistance in two cases which are typical of several application scenarios:

- Case 1: when $\eta_r > 1$, as for example in the case of oil droplets dispersed in water;
- Case 2: when $\eta_r << 1$, as for example in the case of nitrogen bubbles dispersed in water.

Case 1 $\eta_r > 1$: in this case the resistance of a Pipe containing droplets can be approximated by [26, 38]:

$$R^{'} = R(\eta_r\phi + 1 - \phi) = \zeta L_C \mu_c (\eta_r\phi + 1 - \phi)/w, \tag{5.9}$$

where $\zeta = \frac{\alpha}{\mu_c}$ and α is the expression defined in (5.6). Accordingly, we must guarantee that the following relationships hold

$$\begin{cases} L_2 < L_1 \\ \zeta[\mu_c L_2 + L_D(\mu_d - \mu_c)] > \zeta \mu_c L_1. \end{cases} \tag{5.10}$$

As a consequence the MNI design must satisfy the following condition:

$$0 < L_1 - L_2 < L_D\Big(\frac{\mu_d}{\mu_c} - 1\Big). \tag{5.11}$$

Case 2 $\eta_r << 1$: in this case the term $\eta_r\phi$ in the eq. (5.8) can be neglected, whereas $f(\eta_r)$ can be approximated as $f(\eta_r) \simeq 1$. Accordingly, if we define R_D as in [38, 40]

$$R_D = 3.15\frac{\sigma}{h}Ca^{2/3}\frac{1}{U \cdot w \cdot h}, \tag{5.12}$$

where U is the droplet velocity, then the hydrodynamic resistance can be approximated as follows:

$$R' \simeq R(1-\phi) + nR_D. \tag{5.13}$$

If there is only one droplet in the channel, that is, $n = 1$, then (5.13) can be rewritten as

$$R' \simeq \alpha\left[L_C - L_D + \frac{3.15 \cdot (1 - 0.63h/w)}{12}Ca^{-1/3}h\right]/w. \tag{5.14}$$

In the following we set $h/w = 1/2$. Therefore, in the above equation it should be $L_D < 0.18Ca^{-1/3}h$ so that $R' > R = \alpha L_c$; otherwise the channel resistance would decrease in spite of the presence of a droplet in the Pipe, as experimentally observed.

Finally, by imposing that the two Pipes 1 and 2 have the same h and w and only differ for their length, the conditions we are looking for, that is $R_2 < R_1$

and $R_2' > R_1$ can be equivalently rewritten as

$$\begin{cases} L_2 < L_1 \\ \alpha(L_2 - L_D + 0.18Ca^{-1/3}h) > \alpha L_1. \end{cases} \tag{5.15}$$

So it follows that the MNI design must satisfy the following relationship:

$$0 < L_1 - L_2 < 0.18Ca^{-1/3}h - L_D. \tag{5.16}$$

5.3 Further design guidelines

In this section we provide other guidelines which should be considered while designing the HCN components dealing with addressing.

As a first consideration, droplets break up at the bifurcation point B must be prevented. To this purpose, the following condition must hold [41]:

$$L_D < \pi w, \tag{5.17}$$

where L_D is the droplet length and w the channel width. Also, observe that the distance between consecutive droplets changes as they traverse different MNIs. Such changes should be considered while designing the HCN. Suppose that the distance between two droplets entering the i-th MNI is $D_{HP}^{(i)}$ and suppose that the second droplet will follow the first one in Pipe 2. Furthermore, let us call v the velocity of the droplets in the Pipe leading to the bifurcation point B and v_2 the velocity of the droplets in Pipe 2. The distance between the two droplets when they leave the i-th MNI (which we denote as $D_{HP}^{(i+1)}$) will be equal to

$$D_{HP}^{(i+1)} = v_2 \cdot \frac{D_{HP}^{(i)}}{v}. \tag{5.18}$$

The velocities v and v_2 are proportional to the flow rate in the corresponding Pipes; specifically, the following relationship holds:

$$Q_2 \simeq \frac{L_1}{L_1 + L_2} \cdot Q. \tag{5.19}$$

If we use (5.19) in (5.18), we obtain

$$D_{HP}^{(i+1)} \simeq D_{HP}^{(i)} \frac{L_1}{L_1 + L_2}. \tag{5.20}$$

Accordingly, if the microrouter μR sets the distance between the header and payload droplets to D_{HP}, at the entrance of the i-th MNI such distance will be

$$D_{HP}^{(i)} \simeq D_{HP}^{(1)} \cdot \prod_{j=1}^{i-1} \frac{L_1^{(j)}}{L_1^{(j)} + L_2^{(j)}}. \tag{5.21}$$

In the following we will analyze the impact of the number of elements in the HCN on the performance. To this purpose note that in our design $L_1^{(j')} = L_1^{(j'')}$ and $L_2^{(j')} = L_2^{(j'')} \; \forall \; j', j''$. Let us define β as

$$\beta = (L_1^{(j)} + L_2^{(j)})/L_1^{(j)}. \tag{5.22}$$

Accordingly, (5.21) can be rewritten as

$$D_{HP}^{(i)} \simeq D_{HP}^{(1)} \cdot (1/\beta)^{i-1}. \tag{5.23}$$

In order to send a droplet to the i-th element $E_i^{(\Sigma)}$, the microrouter μR must set the distance between the header and payload droplets in such a way that:

$$\begin{cases} D_{HP}^{(j)} > \beta \cdot L_2 & \text{for } j < i. \\ D_{HP}^{(j)} < \beta \cdot L_2 & \text{for } j \geq i. \end{cases} \tag{5.24}$$

By exploiting (5.23) in the relationships given in (5.24), we obtain that the distance between the header and payload droplet set by microfluidic router μR must be such that

$$\beta^{i-1}L_2 < D_{HP}^{(1)} < \beta^i L_2 \quad \text{if } i > 1. \tag{5.25}$$

It follows that the average value of the distance between the header and payload droplet at the transmitter is approximately

$$E\{D_{HP}^{(1)}\} \simeq \frac{1}{M}\sum_{i=1}^{M}\beta^{i-1}L_2 \simeq \frac{\beta^M - 1}{\beta M \log(\beta)}. \tag{5.26}$$

Note that (5.26) has been obtained by assuming that payload droplets are sent to all elements with equal probability and by approximating the sum with the integral. The time required to transmit the header and payload droplets is proportional to $E\{D_{HP}^{(1)}\}$; thus, the throughput of the system varies proportionally to M/β^M. While this behavior may raise scalability concerns, we note that in the mid term HCN will be characterized by rather small values of the number of elements M, and will not have strict requirements in terms of throughput.

CHAPTER

SIX

EXPERIMENTATION

Finally, we have realized a prototype of the device described so far which is shown in Figure 6.1. Microfluidic devices are fabricated in poly(dimethylsiloxane) (PDMS) polymer according to the fast prototyping technique described in [42]. The device includes a T-shaped droplet generator (see Figure 6.1(c)) where the stream of dispersed phase that flows from the vertical channel is sheared by the continuous phase that flows from the horizontal channel. The fluids we have used are a fluorinated oil, FC-3283 ($\mu_c = 1.3$ mPa·s, $\rho_c = 1820$ kg/m^3) and an aqueous dye ($\mu_d = 1$ mPa·s, $\rho_d = 1000$ kg/m^3). A surfactant (PFO) is added to the continuous phase to lower the interfacial tension facilitating droplet formation and stabilization of the emulsion.

The two fluids were injected in the micro-channels by syringe pumps at $Q_d = 0.2$ μL/min and $Q_c = 8$ μL/min.

The distance between droplets has been adjusted by changing the rates of flow of the dispersed phase and the continuous phase.

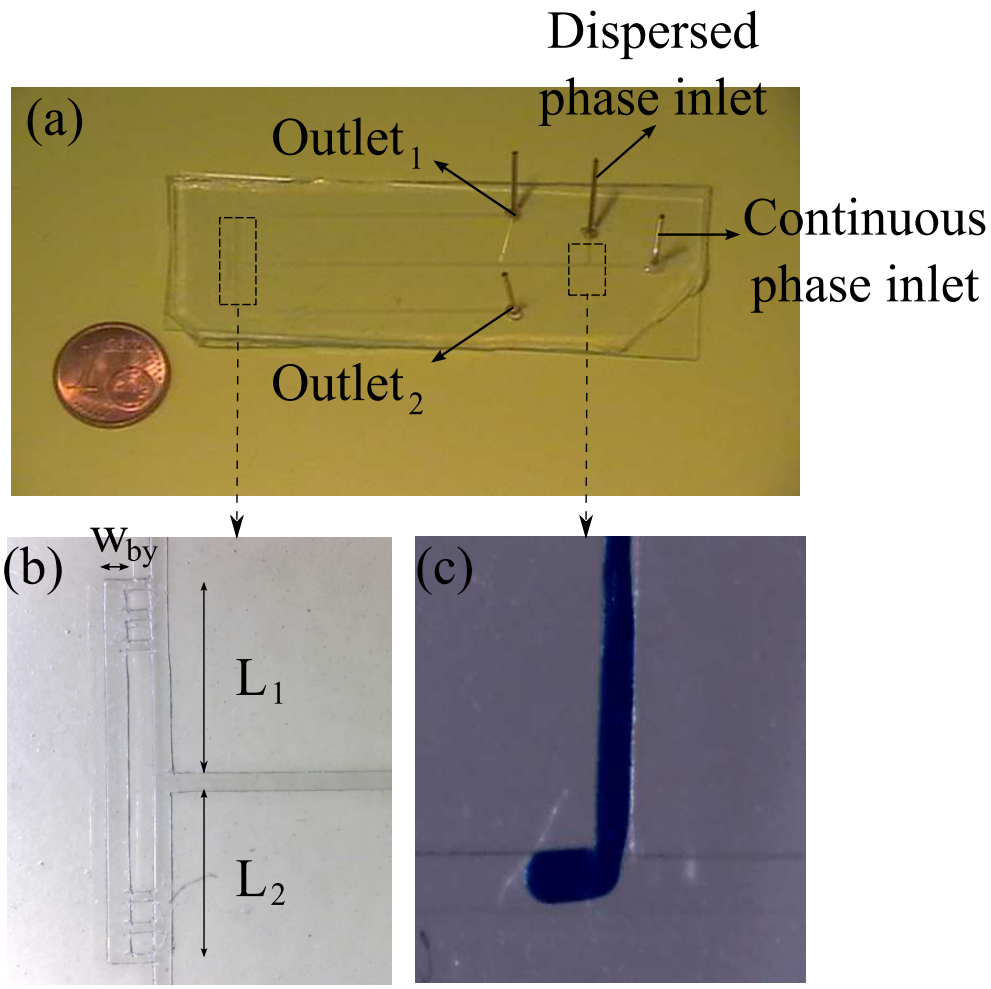

Figure 6.1: Prototype of the HCN addressing device.

In Figures 6.2 we show two snapshots representing:

- the situation before the header droplet arrives at the bifurcation point B (Figure 6.2a). Note that the distance between the header droplet and the payload droplet is such that the header droplet is still inside Pipe 2 when the payload droplet arrives at the bifurcation;
- the situation after the payload droplet leaves the bifurcation point B (Figure 6.2b). Note that the payload droplet has entered Pipe 1, as expected.

In Figures 6.3 we show two snapshots representing:

- the situation before the header droplet arrives to the bifurcation point B (Figure 6.3a). Note that the distance between the header droplet and the payload droplet is such that the header droplet has already left Pipe 2 when the payload droplet arrives at the bifurcation point B.
- the situation after the payload droplet leaves the bifurcation point B (Figure 6.3b). Note that the payload droplet has entered Pipe 2, as expected.

Concluding, we observe that experimental results fit what was obtained through simulations. This confirms the feasibility of designing innovative purely Hydrodynamic Controlled Microfluidic Networks.

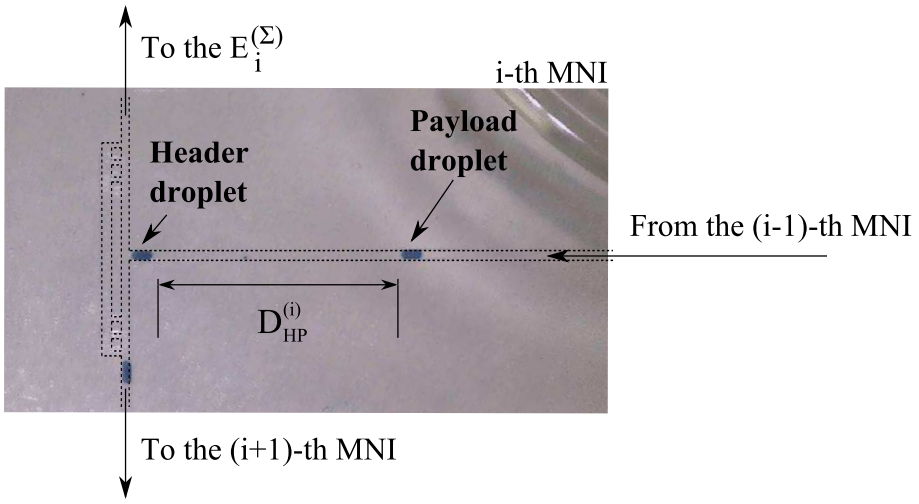

(a) Before the header droplet arrives at *B*.

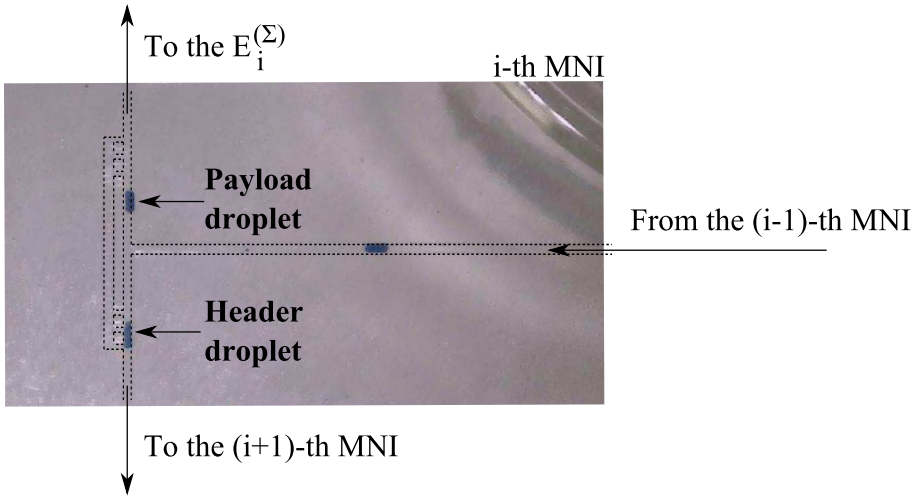

(b) After the payload droplet leaves *B*.

Figure 6.2: Experimental results for the case when the payload droplet enters Pipe 1.

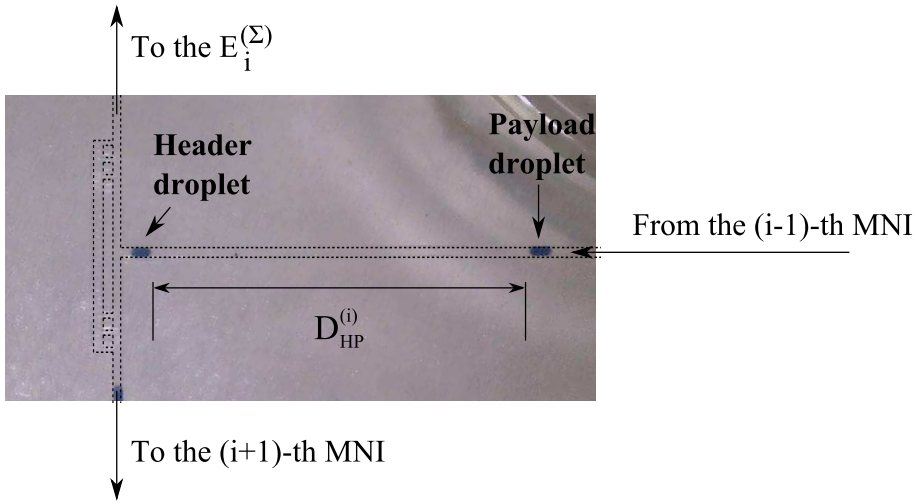

(a) Condition before the header droplet arrives at *B*.

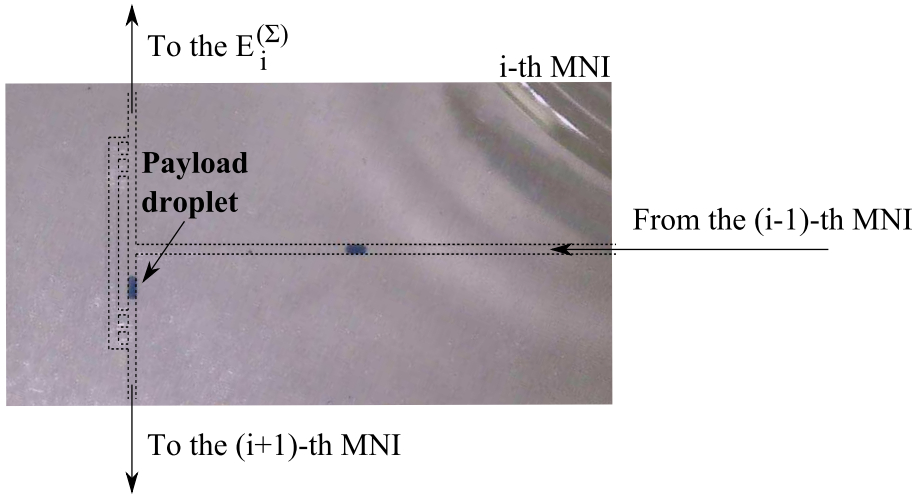

(b) Condition after the payload droplet leaves *B*.

Figure 6.3: Experimental results for the case when the payload droplet enters Pipe 2.

CHAPTER

SEVEN

VALIDATION THROUGH SIMULATION

In this chapter we report the simulation results obtained to assess both the MNI receiving functionalities and its design as described in Chapter 5.

For worth of clarity and brevity we have chosen to report only the simulation results obtained upon considering two MNIs connected as depicted in Figure 7.1.[1] This 3D geometry was simulated using the computational fluid dynamics software OpenFOAM [28]. As we already explained, the bypass channel is a crucial element in the circuit. Note that it must be large enough to guarantee very low hydrodynamic resistance while it must be designed in such a way that droplets do not enter it. In Figure 7.2 we show a zoomed view of the portion of the bypass channel attached to the rest of the circuit, i.e. point *A* in Figure 5.1. The connection consists of a pillar array which prevents droplets from entering the bypass. In Table 7.1 we give the values of the parameters characterizing the geometry used in Figure 7.1.

[1] We omitted here the results in case of more than two MNIs only because more complex effects are met which cannot be intuitively understood as in case of only two MNIs.

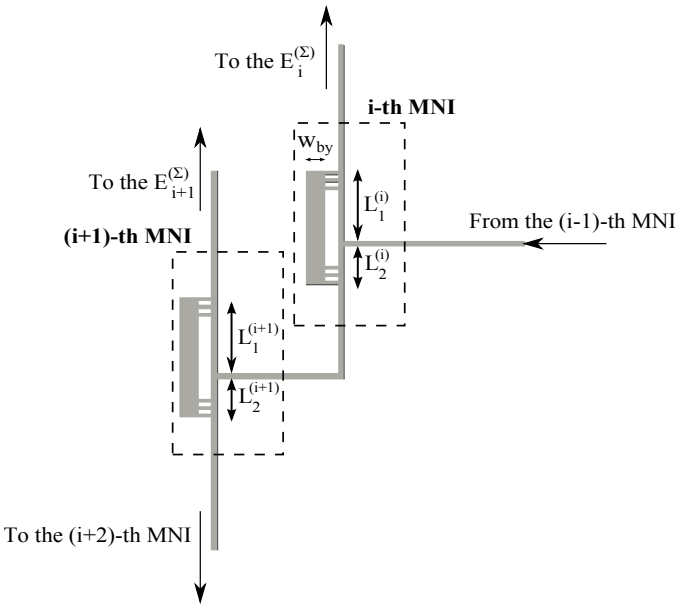

Figure 7.1: Configuration considered for simulations.

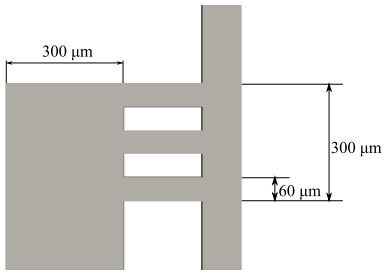

Figure 7.2: Zoomed view of the connection between the bypass channel and the rest of the circuit.

Parameter	w	w_{by}	$L_1^{(i)}$	$L_2^{(i)}$	$L_1^{(i+1)}$	$L_2^{(i+1)}$	h
Value	100 μm	300 μm	1200 μm	600 μm	1200 μm	600 μm	33 μm

Table 7.1: Parameters characterizing the geometry illustrated in Figure 7.1.

For the sake of conciseness, in these simulations we only illustrate the case in which there are oil droplets dispersed in water continuous phase. Accordingly, the viscosities of the dispersed and continuous phases are $\mu_c = 1$ mPa $\cdot$ s and $\mu_d = 10$ mPa $\cdot$ s, respectively. The parameters characterizing the geometry given in Figure 7.1 must satisfy eq. (5.11), where $L_D = 150$ μm.

By using the values given in Table 7.1 we verify that

$$0 < L_1^{(i)} - L_2^{(i)} = L_1^{(i+1)} - L_2^{(i+1)} = \\ = 600 \cdot 10^{-6} < L_D \left(\frac{\mu_d}{\mu_c} - 1 \right) = 1.35 \cdot 10^{-3}.$$

We have considered two cases. In the first case, the payload droplet must be delivered to $E_i^{(\Sigma)}$, whereas in the second case the payload droplet must be delivered to $E_{i+1}^{(\Sigma)}$.

Accordingly, in the first case the distance between the droplets entering the i-th MNI must be such that when the payload droplet arrives at the bifurcation point the header droplet is still in Pipe 2. To this end, such distance $D_{HP}^{(i)}$ must satisfy the following relationship:

$$D_{HP}^{(i)} < \frac{L_1^{(i)} + L_2^{(i)}}{L_1^{(i)}} \cdot L_2^{(i)} - \delta_{\text{Margin}} = 800 \quad \mu\text{m}, \tag{7.1}$$

where δ_{Margin} is a confidence margin utilized to absorb fluctuations in the actual value of the distance between the header and the payload droplets at

the receiving MNI which could cause errors in the delivery of the payload droplet. The value of δ_{Margin} must be set by considering that the distance between droplets changes as they move forward in the microfluidic channels as clarified by (4.25). In our simulations we have chosen $\delta_{\text{Margin}} = 100\ \mu\text{m}$ and $D_{HP}^{(i)} = 600\ \mu\text{m}$ which satisfy the relationship in (7.1).

We show two snapshots of the simulation output representing:

- the situation immediately before the header droplet arrives at the bifurcation point B of the i-th MNI (see Figure 7.3a);

- the situation immediately after the payload droplet left the bifurcation point B of the i-th MNI (see Figure 7.3b).

In Figure 7.3a we observe that the distance $D_{HP}^{(i)}$ satisfies the condition in (7.1), whereas in Figure 7.3b we observe that the payload droplet enters the Pipe leading to $E_i^{(\Sigma)}$. In this case the header droplet will be eliminated by the sink at the end of the HCN.

In the second case, in order for the payload droplet to go towards $E_{i+1}^{(\Sigma)}$, we must guarantee that:

- the distance between the header droplet and the payload droplet before they arrive at the bifurcation point B of the i-th MNI, $D_{HP}^{(i)}$, must be larger than $[(L_2^{(i)} + L_1^{(i)})/L_1^{(i)}] \cdot L_2^{(i)} + \delta_{\text{Margin}}$;

- the distance between the header and the payload droplets before they arrive at the bifurcation point B of the $(i+1)$-th MNI, $D_{HP}^{(i+1)}$, must be smaller than $[(L_1^{(i+1)} + L_2^{(i+1)})/L_1^{(i+1)}] \cdot L_2^{(i+1)} - \delta_{\text{Margin}}$.

By recalling that $D_{HP}^{(i+1)} \approx D_{HP}^{(i)} \cdot L_1^{(i)} / (L_1^{(i)} + L_2^{(i)})$ we obtain

$$\begin{aligned} &\frac{L_1^{(i)} + L_2^{(i)}}{L_1^{(i)}} L_2^{(i)} + \delta_{\text{Margin}} < D_{HP}^{(i)} < \\ &< \frac{L_1^{(i)} + L_2^{(i)}}{L_1^{(i)}} \cdot \frac{L_1^{(i+1)} + L_2^{(i+1)}}{L_1^{(i+1)}} L_2^{(i+1)} - \delta_{\text{Margin}}. \end{aligned} \tag{7.2}$$

Therefore we have set $D_{HP}^{(i)} = 1.1$ mm, which satisfies the condition in (7.2), and we represent the corresponding simulation results in Figure 7.4b. More specifically, in the above figure, we show three snapshots of the simulation output representing:

- the situation immediately before the header droplet arrives at the bifurcation point B of the i-th MNI (see Figure 7.4a);
- the situation immediately after the payload droplet leaves the bifurcation point B of the i-th MNI (see Figure 7.4b);
- the situation immediately after the payload droplet leaves the bifurcation point B of the $(i+1)$-MNI (see Figure 7.4c).

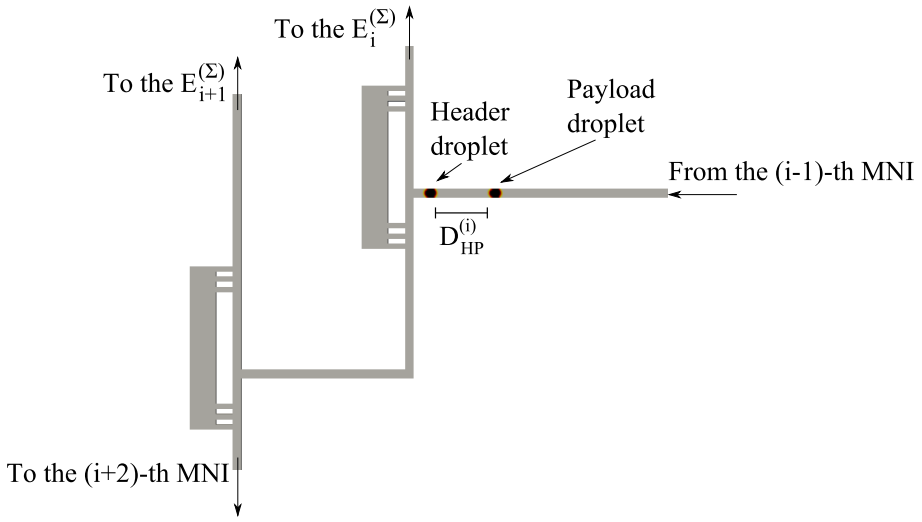

(a) Condition before the header droplet arrives at *B*.

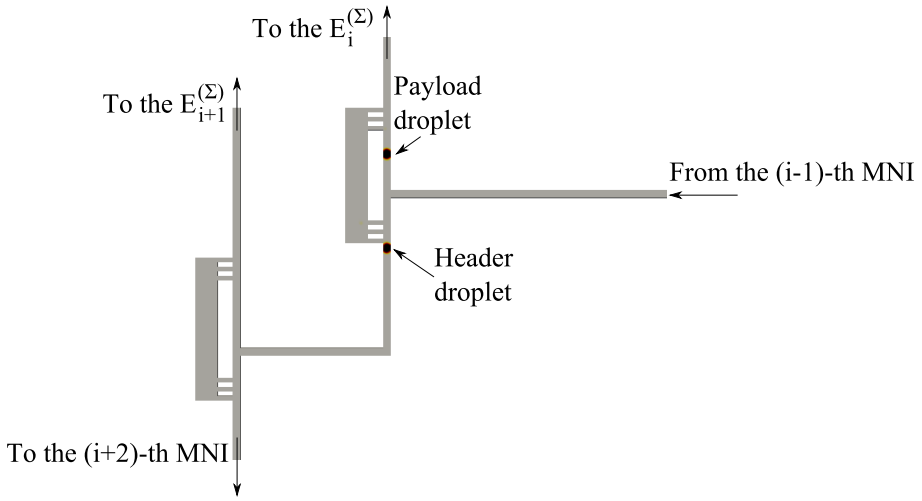

(b) Condition after the payload droplet leaves *B*.

Figure 7.3: Simulation results for the case in which the payload droplet is addressed to the i-th element $E_i^{(\Sigma)}$.

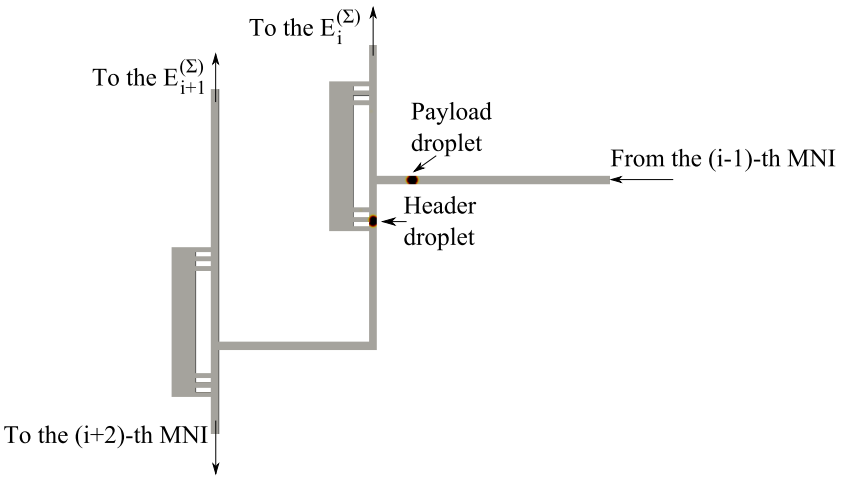

(a) Condition before the payload droplet arrives at the point *B* of the *i*-th MNI.

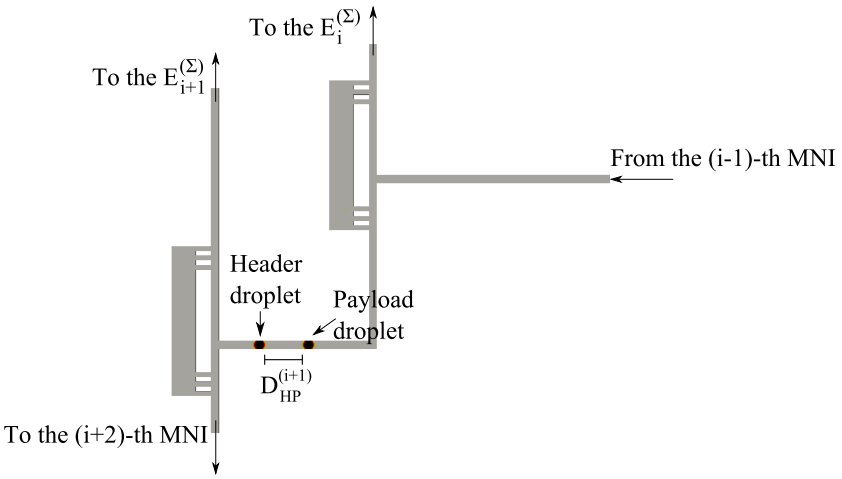

(b) Condition after the payload droplet leaves the point *B* of the *i*-th MNI.

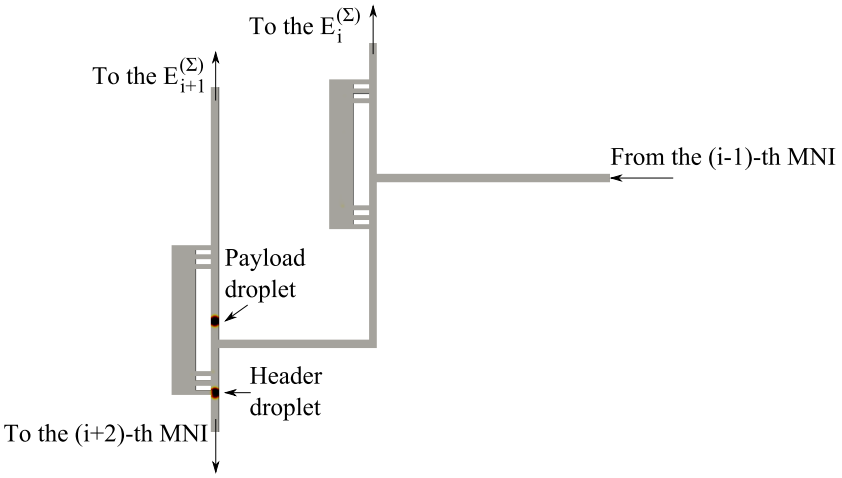

(c) Condition after the payload droplet leaves the point *B* of the $(i+1)$-th MNI.

Figure 7.4: Simulation results for the case in which the payload droplet is addressed to the $(i+1)$-th element $E_{i+1}^{(\Sigma)}$.

CHAPTER

EIGHT

CONCLUSIONS

The incessant search of new solutions for the monitoring and care of human health has been the driver for large research efforts in communications and networking [43, 44]. Furthermore, it has fostered the introduction of communication and networking solutions in several unconventional contexts [45–47].

In this thesis we have proposed a new paradigm of computing denoted as Networked Lab-on-a-Chip (NLoC). It is associated to the use of networking functionalities in microfluidic systems which exploit droplets and/or bubbles to transfer information. Numerous application scenarios can be envisaged, specifically in the context of medical scenarios. Other challenging applications are related, for example, to use of *Ecobots* [48–51] i.e. robots that are supplied by batteries which convert mixtures of organic substances into electricity. To this purpose chemical mixtures need to be delivered from different parts of the robot to the devices which convert food in electricity; so an appropriately designed network of LoCs should dispatch food by means of a fluid carrier. Accordingly we have identified the required functions at a NLoC,

proposed a suitable system architecture, and investigated the related physical level design aspects, such as channel characterization, information representation and information capacity. We have identified the design rules for both the architecture and functionalities to be implemented. In particular encoding and switching functions have been proposed, analyzed, and assessed through simulations. Finally, a prototype has been realized of a pure microfluidic switch. Results of our tests have confirmed the feasibility of this new paradigm.

BIBLIOGRAPHY

[1] Little things factory, 2012.

[2] R. Dangla, F. Gallaire, and C. Baroud, "Microchannel deformations due to solvent-induced pdms swelling," *Lab Chip*, vol. 10, no. 21, September 2010.

[3] C. N. Baroud, F. Gallaire, and R. Dangla, "Dynamics of microfluidic droplets," *Lab Chip*, vol. 10, no. 16, June 2010.

[4] C. N. Baroud, M. Robert de Saint Vincent, and J.-P. Delville, "An optical toolbox for total control of droplet microfluidics," *Lab Chip*, vol. 7, no. 8, June 2007.

[5] V. Ananthanarayanan and W. Thies, "Towards a high-level programming language for standardizing and automating biology protocols," *International Workshop on Biodesign Automation*, July 2009.

[6] B. Mosadegh, C.-H. Kuo, Y.-C. Tung, Y.-s. Torisawa, T. Bersano-Begey, H. Tavana, and S. Takayama, "Integrated elastomeric components for

autonomous regulation of sequential and oscillatory flow switching in microfluidic devices," *Nat. Phys.*, vol. 6, no. 6, July 2006.

[7] G. M. Whitesides, "The origins and the future of microfluidics," *Nature*, vol. 442, no. 7101, July 2006.

[8] M. J. Fuerstman, P. Garstecki, and G. M. Whitesides, "Coding/decoding and reversibility of droplet trains in microfluidic networks," *Science*, vol. 315, no. 5813, February 2007.

[9] M. D. Behzad, H. Seyed-allaei, and M. R. Ejtehadi, "Simulation of droplet trains in microfluidic networks," *Phys. Rev. E*, vol. 82, no. 3, April 2009.

[10] G. Cristobal, J.-P. Benoit, M. Joanicot, and A. Ajdari, "Microfluidic bypass for efficient passive regulation of droplet traffic at a junction," *App. Phys. Lett.*, vol. 89, no. 3, July 2006.

[11] E. D. Leo, L. Galluccio, A. Lombardo, and G. Morabito, "Networked labs-on-a-chip (nloc): Introducing networking technologies in microfluidic systems," *Nano Comm. Net.*, vol. 3, no. 4, December 2012.

[12] E. De Leo, L. Galluccio, A. Lombardo, and G. Morabito, "On the feasibility of using microfluidic technologies for communications in labs-on-a-chip," in *IEEE International Conference on Communications (ICC)*, June 2012.

[13] E. De Leo, L. Galluccio, A. Lombardo, and G. Morabito, "Communications and networking in labs-on-a-chip systems," in *GTTI*, June 2012.

[14] E. De Leo, L. Donvito, L. Galluccio, A. Lombardo, G. Morabito, and L. M. Zanoli, "Design and assessment of a pure hydrodynamic microfluidic switch," in *IEEE ICC-CT*, June 2013.

[15] E. De Leo, L. Donvito, L. Galluccio, A. Lombardo, G. Morabito, and L. M. Zanoli, "Microfluidic networks: design and test of a pure hydrodynamic switching function," in *IEEE ICC - Monacom Workshop*, June 2013.

[16] E. De Leo, L. Donvito, L. Galluccio, A. Lombardo, G. Morabito, and L. M. Zanoli, "Networked lab-on-a-chip: Enhancing locs through microfluidic communications and networking," in *IEEE INFOCOM - Student Poster*, April 2013.

[17] E. De Leo, L. Donvito, L. Galluccio, A. Lombardo, G. Morabito, and L. M. Zanoli, "Communications and switching in microfluidic systems: Pure hydrodynamic control for networking labs-on-a-chip," *Transactions on Communications*, 2013. to appear.

[18] N.-T. Nguyen and S. T. Wereley, *Fundamentals and applications of Microfluidics*. Oxford Master Series In Condensed Matter Physics, Artechhouse, 2006.

[19] H. Bruus, *Theoretical Microfluidics*. Oxford Master Series In Condensed Matter Physics, Oxford University Press, 2007.

[20] O. Cybulski and P. Garstecki, "Dynamic memory in a microfluidic system of droplets traveling through a simple network of microchannels," *Lab Chip*, vol. 10, no. 4, December 2009.

[21] S.-Y. Teh, R. Lin, L.-H. Hung, and A. P. Lee, "Droplet microfluidics," *Lab Chip*, vol. 8, no. 2, January 2008.

[22] M. Prakash and N. Gershenfeld, "Microfluidic bubble logic," *Science*, vol. 315, no. 5813, February 2007.

[23] M. Hashimoto, J. Feng, R. L. York, A. K. Ellerbee, G. Morrison, S. W. Thomas III, L. Mahadevan, and G. M. Whitesides, "Infochemistry: Encoding information as optical pulses using droplets in a microfluidic device," *Journ. of the Amer. Chem. Soc.*, vol. 131, no. 34, August 2009.

[24] W. Engl, M. Roche, A. Colin, P. Panizza, and A. Ajdari, "Droplet traffic at a simple junction at low capillary numbers," *Phys. Rev. Lett.*, vol. 95, no. 20, November 2005.

[25] M. Schindler and A. Ajdari, "Droplet traffic in microfluidic networks: A simple model for understanding and designing," *Phys. Rev. Lett.*, vol. 100, no. 4, January 2008.

[26] F. Jousse, G. Lian, R. Janes, and J. Melrose, "Compact model for multiphase liquid-liquid flows in micro-fluidic devices," *Lab Chip*, vol. 5, no. 6, March 2005.

[27] COMSOL software, 2012.

[28] OpenFOAM software, 2012.

[29] SGI corporation, 2012.

[30] W. J. Dally and B. Towles, "Route packets, not wires: On-chip inteconnection networks," in *DAC '01: Proceedings of the 38th Conference on Design Automation*, 2001.

[31] D. W. M. Marr and T. Munakata, "Micro/nanofluidic computing," *Communications of the ACM*, vol. 50, no. 9, September 2007.

[32] S. Haykin, *Communication Systems, 3Rd Ed.* Wiley Eds., 2008.

[33] M. Belloul, L. Courbin, and P. Panizza, "Droplet traffic regulated by collisions in microfluidic networks," *Soft Matter*, vol. 7, no. 19, August 2011.

[34] K. V. Srinivas, A. W. Eckford, and R. S. Adve, "Molecular communication in fluid media: The additive inverse gaussian noise channel," *IEEE Transactions on Information Theory*, vol. 58, no. 7, July 2012.

[35] R. Raj, N. Mathur, and V. V. Buwa, "Numerical simulations of liquid-liquid flows in microchannels," *Industrial & Engineering Chemistry Research*, vol. 49, no. 21, August 2010.

[36] T. Glawdel and C. Ren, "Global network design for robust operation of microfluidic droplet generators with pressure-driven flow," *Microfluidics and Nanofluidics*, vol. 13, no. 3, September 2012.

[37] H. Wong, C. J. Radke, and S. Morris, "The motion of long bubbles in polygonal capillaries. part 2. drag, fluid pressure and fluid flow," *Journ. of Fluid Mechanics*, vol. 292, June 1995.

[38] F. Jousse, R. Farr, D. R. Link, M. J. Fuerstman, and P. Garstecki, "Bifurcation of droplet flows within capillaries," *Phys. Rev. E*, vol. 74, no. 3, September 2006.

[39] S. R. Hodges, O. Jensen, and J. M. Rallison, "The motion of a viscous drop through cylindrical tube," *Journ. of Fluid Mechanics*, vol. 501, February 2004.

[40] P. Parthiban and S. A. Khan, "Filtering microfluidic bubble trains at a symmetric junction," *Lab Chip*, vol. 12, no. 3, February 2012.

[41] D. R. Link, S. L. Anna, D. A. Weitz, and H. A. Stone, "Geometrically mediated breakup of drops in microfluidic devices," *Phys. Rev. Lett.*, vol. 92, no. 5, February 2004.

[42] L. Zanoli, M. Licciardello, R. D'Agata, C. Lantano, A. Calabretta, R. Corradini, R. Marchelli, and G. Spoto, "Peptide nucleic acid molecular beacons for the detection of PCR amplicons in droplet-based microfluidic devices," *Anal. and Bioanal. Chemistry*, vol. 405, no. 2-3, January 2013.

[43] H. Alemdar and C. Ersoy, "Wireless sensor networks for healthcare: A survey," *Computer networks*, vol. 54, no. 15, October 2010.

[44] L. Galluccio, T. Melodia, S. Palazzo, and G. E. Santagati, "Challenges and implications of using ultrasonic communications in intra-body area networks," in *IEEE WONS*, January 2012.

[45] I. Akyildiz, J. Jornet, and M. Pierobob, "Nanonetworks: A new frontier in communications," *Communications of the ACM*, vol. 54, no. 11, November 2011.

[46] L. Galluccio, S. Palazzo, and G. E. Santagati, "Characterization of signal propagation in neuronal systems for nanomachine-to-neurons communications," in *IEEE Infocom - Monacom Workshop*, April 2011.

[47] L. Galluccio, S. Palazzo, and G. E. Santagati, "Capacity analysis for signal propagation in nanomachine-to-neuron communications," in *IEEE ICC - Monacom Workshop*, June 2012.

[48] I. Ieropoulos, J. Greenman, C. Melhuish, and I. Horsfield, "Ecobot-iii: a robot with guts," *proc. of Alife XII conference, Odense, Denmark*, August 2010.

[49] I. Ieropoulos, J. Greenman, and C. Melhuish, "Microbial fuel cells based on carbon veil electrodes: Stack configuration and scalability," *Intern. Journ. of Energy Research*, vol. 32, no. 13, April 2008.

[50] I. Ieropoulos, C. Melhuish, and J. Greenman, "Artificial gills for robots: Mfc behaviour in water," *Bioinspiration and Biomimetics*, vol. 2, no. 3, June 2007.

[51] C. Melhuish, I. Ieropoulos, J. Greenman, and I. Horsfield, "Energetically autonomous robots: Food for thought," *Autonomous Robots*, vol. 21, no. 3, May 2006.